Experimental investigation and model development for thermal conductivity of glycerol-MgO nanofluids

Ntumba Tshimanga, Mohsen Sharifpur and Josua P. Meyer

Nanofluids Research Laboratory, Department of Mechanical and Aeronautical Engineering

 University of Pretoria, Pretoria, South Africa

This paper presents experimental and theoretical determination of the effective thermal conductivity of three magnesium oxide (MgO) nanoparticles of different sizes dispersed in glycerol. The glycerol-based nanofluids were prepared at volume fractions ranging from 0.5% to 4% and no surfactant. The nanoparticles were dispersed and deagglomerated for two hours using an ultrasonic probe. The effective thermal conductivity of nanofluids was measured from 20 ℃ to 45 ℃ using a thermal conductivity analyser. The experimental results show an increase in the thermal conductivity of MgO-glycerol nanofluids with increasing volume fraction of nanoparticles. The thermal conductivity ratio is unaffected as the temperature increases. In the given volume fraction and temperature range, the thermal conductivity ratio of MgO-glycerol nanofluids decreases with increasing particle size. The obtained experimental data were also compared with some existing theoretical and empirical models that may work for glycerol-based nanofluids. The comparison of experimental data with these available models shows that the data does not agree with the models. Therefore, a new empirical correlation was developed for the MgO-glycerol nanofluids.

Address correspondence to: Mohsen Sharifpur, Department of Mechanical and Aeronautical Engineering, University of Pretoria, Pretoria, South Africa
Email: mohsen.sharifpur@up.ac.za
Tel: +27 12 420 2448
Fax: +27 12 420 6632

INTRODUCTION

Investigation into finding a heat transfer fluid with higher performance than conventional liquids (water, ethylene glycol, engine oil, transformer oil, etc.) is a challenge for many industries. Choi [1] has proposed nanofluids as an efficient heat transfer fluid since 1995. Afterwards, a large number of experimental and theoretical investigations were performed to study the properties of nanofluids prepared with various conventional fluids and different nanoparticles. Numerous experimental investigations on nanofluids show that effective thermal conductivity ratio (TCR) depends on many parameters, including particle volume fraction, nanoparticle size, nanoparticle shape, nanoparticle material, amount and type of surfactants, temperature, thickness of the nanolayer, thermal conductivity of the nanolayer, thermal conductivity of the base fluid, thermal conductivity of the nanoparticles and the pH of nanofluids [2-10].

Several empirical and theoretical correlations exist to model the thermal conductivity of nanofluids. Experimental investigations show either an agreement or disagreement with the theoretical studies, and whether the predictions of the existing mathematical models for the effective thermal conductivity of nanofluids [4, 10-15] are valid or not. The nanofluids that contain a few percent volume fraction of carbon nanotube (0.2% to 1%) showed a high enhancement of thermal conductivity, ranging from 20% to 150% compared to copper monoxide, which increased from 5% to 22% for a volume fraction ranging from 1% to 4% or 0.1% to 0.3% of copper metallic nanoparticles from 10% to 40% [16, 17].

From recent literature, it is noticed that nanoparticle volume fraction is the most investigated parameter in this field. Mostly, researchers find a linear relationship between the nanoparticle volume fraction and the effective thermal conductivity ratio [8, 13, 18-20]. However, some

researchers reported a non-linear relationship, especially at low volume fraction [17, 21]. Several researchers have also investigated the effect of temperature on the thermal conductivity ratio of both water-based and ethylene glycol and water-based nanofluids. They reveal that the thermal conductivity increases with increasing temperature [8, 13, 22].

Water is one of the best choices for liquid cooling applications due to its availability, low viscosity, acceptable heat capacity and thermal conductivity. However, in the cold regions, water alone is less desired because of its freezing point at 0 ˚C. Instead, an ethylene glycol and water mixture (60:40 wt.) is widely used as the heat transfer fluid in building heating systems, geothermal heat and cooling systems, automobiles and heat exchangers [13].

Glycerol is common as an additive in many creams and lotions to keep the skin soft and moisturised. It was historically used as an antifreeze for a broad range of mechanical equipment during the winter periods to prevent the freezing of aqueous heat transfer fluids before being replaced by ethylene glycol in the 1930s due to cost considerations.

Nowadays, glycerol, which is more environmentally friendly than ethylene glycol, is being examined by the American Society for Testing and Materials (ASTM) International Committee D15 [23] in order to use in automotive applications. This is due to surplus production of glycerol from biodiesel in the global market since 2004. This situation could affect the cost-effective return of glycerol as an antifreeze. Glycerol is often used as a lubricant, not only because of its high viscosity, but also for its ability to remain fluid at low temperatures. It is also more resistant to oxidation than oil. Glycerol is recommended as a lubricant as opposed to mineral oils for oxygen compressors, pumps and bearings that are exposed to fluids such as gasoline and benzene. It is also recommended where there is contact with lubricants in food, and in the

manufacture of pharmaceuticals and cosmetics where purity is crucial. It is used as a plasticiser of heat casings and special types of papers (glassine and greaseproof paper). Glycerol can also be used in many industries, such as the food, pharmaceutical, chemical, textile and plastic industries [24]. Glycerol is employed as an ingredient in cough medicines, anaesthetics, the treatment of ear infections and bacteriological culture media.

In view of the interest in glycerol, especially in the automotive industry, it was deemed necessary to study the applicability of MgO-glycerol nanofluids for heat transfer applications. To the best of our knowledge, there is no reported data on thermal conductivity of MgO-glycerol nanofluids to date. As a result, the experimental results that elucidate the influencing factors for the thermal conductivity of MgO-glycerol nanofluids are presented in this work. The study aims to estimate the effect of nanoparticle volume fraction, diameter and temperature on the thermal conductivity of stable MgO-glycerol nanofluids. Furthermore, the measured thermal conductivities are compared with the predicted values of available theoretical and empirical models. Consequently, an accurate model for the effective thermal conductivity of MgO-glycerol nanofluids is developed.

EXPERIMENTAL PROCEDURES AND VALIDATION

Materials

Three MgO nanoparticles of different diameters were provided for analysis with factory specifications of 20 nm (S1), 40 nm (S2) and 100 nm (S3). The MgO nanopowder of 100 nm was purchased from Nanostructured and Amorphous Materials Inc. in Houston, Texas. The two other MgO nanoparticles, with average particle sizes of 20 nm and 40 nm, were procured from

US Research Nanomaterials Inc., also in Houston, Texas. Merck Millipore in Darmstadt, Germany, supplied the glycerol (base fluid). Table 1 presents the physicochemical properties of the magnesium oxide nanoparticles [21, 25, 26].

Physical characterisation of nanoparticles

The X-ray fluorescence spectroscopy (XRF), an X-ray powder diffraction (XRD) and combined XRD and XRF were used to determine the physical characterisation of the MgO nanoparticles. The XRD analysis of MgO nanoparticle samples was done using a PANanalytical X'Pert Pro powder diffractometer. The source was Co-Kα radiation of wavelength (λ) = 1.78901 Å, with an acceleration tension of 50 kV and current of 50 mA. The samples were recorded over a 2θ range of 10° to 90° with a scanning rate of 0.02°/s. The instrumentation used for the XRF analysis is an ARL 9400XP spectrometer.

Transmission electron microscopy (TEM) images were acquired with a JEOL JEM–2100F transmission electron microscope. The JEM 2100F works with an accelerating voltage of 200 kV in the range of 50 V/min at variable steps of 2 ppm/min. The JEM 2100F achieves the highest TEM image quality with a point image resolution at 0.23 nm accuracy [27]. TEM image files were analysed using ImageJ, an open-source code written at the US National Institutes of Health. The samples were prepared by dispersing the MgO nanopowder in acetone through ultrasonication for five minutes.

Thermal conductivity measurement

The thermal conductivity data was measured using a handled Decagon KD2 Pro thermal properties analyser. The transient hot-wire source method is based on the principle of measurement of the instrument. The apparatus consists of a handled controller and sensors that operate in the temperature ranges of 0 ˚C to 50 ˚C and -50 ˚C to 150 ˚C, respectively. The device uses a small single needle (KS-1) of 1.3 mm in diameter and 60 mm in length. The apparatus operates with 5% accuracy over the temperature range of 0 ˚C to 50 ˚C for the thermal conductivity range of 0.02 to 2 W/mK. A heater and temperature sensor is inside the probe, which is vertically inserted into the fluid sample. A small amount of heat is applied to the sample for half of the time and the measurements are taken over the full time. The probe's temperature is passed through the heater. Decagon Devices shows that the thermal conductivity is computed using the temperature difference versus time data using a particular algorithm given by Carslaw and Jaeger for infinite source [28]. The KD2 Pro complies with the standards of both ASTM D5334 and Institute of Electrical and Electronics Engineers (IEEE) 442-1981 regulations. Several researchers have successfully used the KD2 Pro thermal analyser [4, 29].

Preparation of nanofluids

Two-step techniques have been applied to prepare nanofluids in this study. Manufacturers first produced the three MgO nanoparticles as dry powders by chemical and/or physical methods. Therefore, the nano-sized powder was dispersed into a glycerol (base fluid) in the second processing step with the help of intensive ultrasonic agitation, high-shear mixing and homogenising.

The MgO-glycerol nanofluids were prepared in a 100 ml beaker. No surfactant or dispersant was considered in the preparation of MgO-glycerol nanofluids for the entire nanoparticle volume fractions ranging from 0.5% to 4%. The nanofluid was ultrasonicated with the S14 sonotrod (UP200S Hielscher of 200 Watts operated at 24 kHz) [30] for two hours in a thermal bath to ensure uniform dispersion of the nanoparticles. The UP200S was regulated to transfer an acoustic irradiation of 75% amplitude at a period of 0.9 sec/sec to nanofluid. A LAUDA ECO RE1225 Silver thermal bath was used to obtain and/or maintain different temperatures of nanofluids during the measurement process. After sonication, the nanofluids were kept still for 30 minutes to minimise the forced convection produced by both the ultrasonicator probe and the thermal bath. The influence of various sonication times (30 minutes, one hour, two hours, three hours and five hours) were investigated on the effective thermal conductivity at both 1% and 4% volume fraction MgO-glycerol nanofluids of three nanoparticle sizes. The results show that the k_{eff} of the three MgO-glycerol nanofluids increases as the sonication time increases up to one hour and becomes almost constant afterwards [31]. Equation (1) was used to determine the volume fraction of nanoparticles ϕ:

$$\phi = \frac{\dfrac{W_{MgO}}{\rho_{MgO}}}{\dfrac{W_{MgO}}{\rho_{MgO}} + \dfrac{W_{Glycerol}}{\rho_{Glycerol}}} \times 100\% \qquad (1)$$

Where $W_{MgO}, W_{Glycerol}, \rho_{MgO}, \rho_{Glycerol}$ are respectively the weight of the MgO nanoparticles, the weight of the glycerol, the density of the MgO nanoparticles and the density of the glycerol.

The nanoparticles were weighed using an Adam HCB1002 electronic balance with an accuracy of ± 0.01 g and then dispersed into the pre-weighed quantity of the base fluid.

Validation of experimental data

The validation of the thermal analyser was done by comparing results obtained from glycerol with available data in the literature [32, 33] for temperatures ranging from 20 ˚C to 45 ˚C. Figure 1 shows that the thermal conductivity values of glycerol measured with the KD2 Pro are in excellent agreement with available data. The majority of the experimental results (99.998%) fall within 2% of the predicted values. Each set of data represents an average of nine measurements for each sample at the same condition. The impact of measurable parameters, such as nanoparticle volume fraction, temperature and size, on the effective thermal conductivity of MgO-glycerol nanofluids is analysed in the next section.

RESULTS AND DISCUSSION

Sample characterisation

Figure 2 represents the TEM image of the three samples of MgO nanoparticles, which are approximately spherical. The images show typical degrees of agglomeration of nanoparticles. Figure 3 summarises the results of nanoparticle size distribution studies using ImageJ software. The particle size data is based on the TEM image analysis of more than 500 particles, which are individually counted. The results indicate that Gaussian profiles are fitted to the three histograms. The average particle diameters and their standard deviations obtained from the TEM images computed were 21.1 ± 4.1 nm for S1, 123.7 ± 45.5 nm for S2 and 103.8 ± 28.1 nm for

S3, of which the accuracy of the TEM images of JEL 2100F is 0.23 nm [27]. S2 is by far more polydisperse than S3. Furthermore, the average particle diameter of S2 is greater than the manufacturer value (40 nm). As the manufacturer does not analyse nanoparticle TEM analysis batch by batch, the variation may occur due to an unforeseen event that can take place in the nanoparticle manufacturing process. Therefore, this report is based on TEM analysis and not the manufacturer's values. Table 2 shows the results of XRF analysis. The results disclose that the MgO and minor impurities predominantly constituted the nanoparticles. Figure 4 gives the typical XRD patterns of the nanoparticle samples. The diffraction peaks of 111, 200, 220 and 311 of both S1 and S3 can be indexed as the cubic structure MgO from the International Center for Diffraction Data (ICDD) database of powder diffraction patterns with PDF number 01-087-0651, while the other small peaks displayed XRD patterns of brucite corresponding to PDF number 01-083-0114. The main peaks of S2 can be indexed to the cubic structure of MgO with PDF file number 01-078-0430.

The mineralogical analysis reveals that both S1 and S2 consist of a mixture of periclase (MgO) and brucite, but with high concentrations of the periclase, while periclase constitutes S3 as shown in Table 2 and Table 3. The agglomeration of crystallites forms the nanoparticle solid powders. The Scherrer equation (2) can approximate the average crystallite size by measuring the broadening of the X-ray diffraction peaks. This equation predicts at best ±10% of the crystallite size, on which the assumption of $K = 1$ is considered [34, 35].

$$d_{crist} = \frac{K\lambda}{\beta \cos \theta} \qquad\qquad (2)$$

Where λ is the wavelength of the X-ray source (1.78901 Å), K is a shape factor varying from 0.62 to 2.08, β is the peak width of the profile at full width at half maximum (FWHM) of crystallite size in radians, and θ is the Bragg angle of the peak in degrees or radians. The shape factor (K) is a numeric value that describes the form of the nanoparticle, type of approach calculation and the size distribution. K is equal to 0.89 and 0.94 for spherical particles with cubic symmetry crystallites determined by integral breadth and FWHM, respectively. In both cases, an approximate value of 1 can also be used [35]. In TEM image analysis, Equation (3) defines the circularity parameter. The circularity value (*circ*) of 1 and approaching 0 refers to the perfect circle and the increasingly elongated shape object, respectively [36].

$$circ = 4\pi \left(\frac{A}{P^2} \right) \qquad\qquad (3)$$

Where A and P are the projected area and outside perimeter of the outline of the nanoparticle, respectively.

The circularity of 21.1 nm, 103.7 nm and 123.7 nm MgO nanoparticles are 0.8, 0.9 and 0.9 respectively. The circularity values of the three nanoparticles indicate that our nanoparticles have a shape closer to the sphere than that of an elongated shape object.

Table 4 summarises the calculated crystal size details and other TEM and XRD. The estimated crystallite sizes are 18 nm to 20 nm for the 21.1 nm MgO, 41 nm to 49 nm for the 123.7 nm MgO, and 41 nm to 48 nm for the 103.8 nm MgO nanoparticles respectively. One can see that they are up to three times smaller than their corresponding average particle sizes. It can be assumed that the 21.1 nm MgO is monocrystalline, while the 123.7 nm MgO and 103.8 nm MgO are polycrystalline. However, the calculation has been done without correction for instrumental stress broadening and any other possible sources of line broadening.

Uncertainty calculation

The uncertainty of experimental results was determined by the measurement errors of the thermal conductivity, temperature and weight. The uncertainty in measurement of thermal conductivity by KD2 Pro is 5%. The accuracy of the weighing scale is 0.01 g between 0.8 g and 55 g. Therefore, at the mean weight of 27.9 g, $\left(\frac{\Delta W}{W}\right) = 0.036\%$. The uncertainty for temperature measurement is 0.01 °C between the 20 °C and 45 °C, $\left(\frac{\Delta T}{T}\right) = 0.03\%$. The uncertainty in TCR (u_{TCR}) is given in equation (4):

$$u_{TCR} = \pm\sqrt{\left(u_{keff} * \frac{\partial TCR}{\partial k_{eff}}\right)^2 + \left(u_{kf} * \frac{\partial TCR}{\partial k_f}\right)^2} \qquad (4)$$

Equation (5) gives the uncertainty of the thermal conductivity (k_{eff} and k_f). Combining all together, the uncertainty in the effective thermal conductivity (k_{eff}) and TCR are 5% and 8.5%, respectively.

$$u_k = \pm\sqrt{\left(\Delta k / k\right)^2 + \left(\Delta T / T\right)^2 + \left(\Delta W / W\right)^2} \qquad (5)$$

Influence of volume fraction on the thermal conductivity

The effective thermal conductivity ratio of the three sets of MgO-glycerol nanofluids as a function of MgO nanoparticle volume fraction between 0.5% and 4% was measured at 20 °C, 25 °C, 30 °C, 35 °C, 40 °C and 45 °C. Figure 5 shows the volume fraction dependence of the effective thermal conductivity ratio of MgO-glycerol nanofluids at maximum temperature. Error bars on the graph indicate standard deviation over five consequent measurements. The use of

MgO nanoparticles dispersed in glycerol yielded higher thermal conductivity than the base fluid. The best-fit curves are provided for visualisation purposes. The thermal conductivity ratio of the three sets of MgO-glycerol nanofluids increases linearly with increasing MgO nanoparticle volume fractions, which agrees with other studies of a broad range of nanofluids [8, 13, 18-20, 37]. The 21.1 nm MgO-glycerol gives the highest values of k_{eff}/k_f, followed by 103.8 nm MgO and 123.7 nm at all ranges of temperature. The experimental data, which is shown in Figure 5, clearly approves the impact of particle size on the k_{eff}/k_f. The k_{eff}/k_f increases with decreasing nanoparticle diameters. The thermal conductivity ratio reaches the maximum of 19%, 17% and 16% for 21.1 nm, 103.8 nm and 123.7 nm MgO-glycerol nanofluids at 45˚C respectively.

The observed enhancement in all nanofluid samples with respect to the volume fraction as depicted in Figure 5 could possibly be explained by one or more mechanisms, including Brownian motion nanoparticle clustering and layering at the solid-liquid interface. The suspended MgO nanoparticles in the glycerol increase the surface area and the heat capacity of the glycerol, and both interaction and collision among MgO nanoparticles are strengthened [38, 39]. The Brownian diffusion coefficient, expressed by the Einstein-Stokes equation, is directly proportional to temperature and reciprocal to both the nanoparticle diameter and the viscosity of the liquid. Nanofluids prepared with smaller nanoparticles will result in more severe collisions among nanoparticles and fluid molecules than the one made with larger-sized nanoparticles. The particle-to-particle interaction increases as the distance between the nanoparticles decreases by increasing the volume fraction of the nanoparticle. The increase in nanoparticle volume fraction intensified the collision and interaction among nanoparticles, diffusion into nanofluid and the heat capacity of the glycerol, enhancing the thermal conductivity of MgO-glycerol nanofluids.

Influence of temperature on the nanofluids' thermal conductivity

The temperature dependence of thermal conductivity was investigated for all three sizes of MgO-glycerol nanofluids. Measurements of four particle volume fractions (0.5%, 1%, 2% and 4%) were made at six different temperatures (20 °C, 25 °C, 30 °C, 35 °C, 40 °C and 45 °C). The results in Figure 6 show that the temperature dependence of the effective thermal conductivity of nanofluids tracks the base fluid (glycerol), but in another level of magnitude. Similar findings were reported for the water-based nanofluids containing Al_2O_3 [18] and ethylene glycol nanofluids containing Al_2O_3, MgO, ZnO, SiO_2 and graphene nanoparticles [3, 18, 40, 41]. Figure 6 clearly demonstrates that the k_{eff} varies significantly with nanoparticle volume fraction for all three samples of nanofluids, but varies slightly with temperature.

Figure 7 plots the thermal conductivity ratio of MgO-glycerol nanofluids at different volume fractions for a temperature ranging from 20 °C to 45 °C. Figure 7 reveals that there is no dependence of k_{eff}/k_f on temperature for all three nanofluid samples. One can also observe that the thermal conductivity ratio varies significantly with an increase in particle volume fraction. The highest value of k_{eff}/k_f is obtained at the maximum volume fraction (4%) and lowest particle size of MgO-glycerol (21.1 nm). No experimental data of the thermal conductivity ratio of MgO-glycerol nanofluids with temperature are available in the literature for comparison with the present experimental data. The findings are consistent with results obtained by Xie *et al*. [21]. They depicted that the effective thermal conductivity of 5% MgO-EG nanofluid varies in the temperature range of 10 ˚C to 60 ˚C, while the k_{eff}/k_f is almost constant. On the contrary, Saleh *et al.* [4], and others [3, 4, 37, 42, 43] have shown recently that the effective thermal conductivity

ratio of nanofluids varies with increasing temperatures. Therefore, the effect of temperature on thermal conductivity ratio depends on the nanofluid characteristics.

Influence of nanoparticle size on the nanofluids' thermal conductivity

In order to assess the influence of the nanoparticle size on the effective thermal conductivity ratio of MgO-glycerol nanofluids, experiments were conducted for different nanoparticle volume fractions (0.5%, 1%, 2% and 4%) at various temperatures (20 °C, 25 °C, 35 °C and 45 °C). Figure 8 shows the influence of diameter on the MgO-glycerol thermal conductivity ratio at room temperature. For the given volume fraction and temperature, the thermal conductivity ratio decreases with increasing particle size. The thermal conductivity ratio of MgO-glycerol nanofluid in the case of the same volume fraction is higher for smaller particle sizes.

The 103.8 nm MgO-glycerol has k_{eff}/k_f values close to 123.7 nm MgO-glycerol nanofluids at almost all temperatures. The possible explanation can be clarified by the Brownian motion theory. The Brownian diffusion coefficient, which is expressed by the Einstein-Stokes equation, is directly proportional to temperature and inversely proportional to both nanoparticle diameter and the liquid's viscosity. Nanofluids prepared with small nanoparticles will result in more severe collisions among nanoparticles and fluid molecules than those prepared with bigger nanoparticles, which leads to better thermal conduction [37, 38]. In addition, the smaller particles exhibit a larger surface area to volume ratio than the bigger particles, which can result in a noticeable enhancement of the effective thermal conductivity [41]. For a given volume fraction, the number of nanoparticles in the glycerol increases as the size of the nanoparticles decreases.

The increase in the number of MgO nanoparticles in the glycerol will intensify the collision and interaction among nanoparticles, diffusion into nanofluid and the heat capacity of the glycerol. Consequently, the thermal conductivity of MgO nanofluid will be improved.

Stability of MgO-glycerol nanofluids

Figure 9 presents the stability of nanofluids relative to the effective thermal conductivity of both 0.5% and 4% volume fraction for MgO-glycerol nanofluids (21.1 nm, 103.8 nm and 123.7 nm). No surfactant has been used in the preparation of the nanofluids. After sonication, the experimental data set for different diameters at each hour up to 48 hours was acquired. For clarity, the data have been plotted at four-hour intervals and the standard deviation of the data has been omitted. The results show no change in effective thermal conductivity with time after nanofluid preparation, as opposed to the results of a study conducted by Xie *et al.* [21] and some other researchers [38]. Xie *et al.* [21] examined the influence of settlement time on the thermal conductivity ratio of MgO-ethylene glycol (5% volume) nanofluids after three hours of sonication. They demonstrated that the thermal conductivity decreases with elapsed time in the first six hours and becomes constant afterwards up to 25 hours; k_{eff}/k_f decreases with less than 3%.

Khedkar *et al.* [38] investigated the influence of elapsed time, from 0 to 30 minutes after 80 minutes of sonication, on the effective thermal conductivity of CuO-monoethylene glycol and CuO-water nanofluids (3% volume fraction). They found that, initially, the thermal conductivity decreases with the time elapsed up to 10 minutes. Afterwards, it is almost unchanged. The same observation was demonstrated for water-based nanofluids [21, 44]. This effect is more noticeable for water-based nanofluids prepared without surfactants than for those prepared with surfactants.

The possible reason why the thermal conductivity of MgO-glycerol nanofluids was not enhanced in the early hours after sonication could be that there was no clustering and settling of nanoparticles [21, 38, 44, 45]. The effective thermal conductivity measurement indicates the stability of MgO-glycerol nanofluids at both small and high volume fractions at room temperature.

Comparison of the thermal conductivity models with experimental data

Existing theoretical and empirical models

There are more than 30 empirical correlations and theoretical models that can be used to estimate the effective thermal conductivity ratio of different nanofluids [46, 47]. None of the empirical correlations and models have been based on the glycerol-based nanofluid data. In this paper, four of the existing models will be used to predict the present experimental data. Maxwell introduced the first simple model of effective thermal conductivity (k_{eff}) for micro or millimetre-sized particles suspended in base fluids [48]:

$$k_{eff} = \frac{k_p + 2k_f + 2(k_p - k_f)\phi}{k_p + 2k_f - (k_p - k_f)\phi} k_f \qquad (6)$$

where k_p is the thermal conductivity of the particle, k_f is the thermal conductivity of the base fluid and ϕ is the volume fraction of the suspension. Maxwell's formula gives an excellent result for well-dispersed non-interacting spherical particles with low particle volume concentrations

and negligible thermal resistance at the particle-fluid interface. The Maxwell model is acceptable when $k_p >> k_f$ and $\varphi \le 1.$.

Bruggeman [11] proposed the implicit formula for the effective thermal conductivity of spherical particles randomly distributed in the base fluid. The model is based on the differential effective medium (DEM) theory to estimate the effective thermal conductivity of composites at low and high particle volume concentrations. The model predicts a good match with some experiment results for low and high solid concentration. However, the Bruggeman model takes into account three important parameters, namely ϕ, k_f and k_p except the particle size (equation (7)). This model gives a similar result as the Maxwell model for low solid concentration. The Bruggeman model gives lower values of thermal conductivity of nanofluids than the experimental data [49].

$$\phi\left(\frac{k_p - k_{eff}}{k_p + 2k_{eff}}\right) + (1-\phi)\left(\frac{k_f - k_{eff}}{k_f + 2k_{eff}}\right) = 0 \tag{7}$$

The effective medium equation [18] predicts the thermal conductivity ratio for highly conducting spherical particles. In this model, the particles are assumed to be immobile.

$$k_{eff} = [1 + 3\phi]k_f \tag{8}$$

In 2011, Corcione [22] developed an empirical correlation, expressed in Equation (9), for predicting the thermal conductivity ratio from the experimental data of nanofluids consisting of alumina, copper oxide, titania and copper nanoparticles suspended in water or EG. The

correlation is valid for nanoparticles in the range of 21 °C to 51 °C, volume fraction 2% to 9% and nanoparticle diameter 10 nm to 150 nm. The correlation was obtained by way of regression analysis with a 1.86% standard deviation of error. The water and EG thermal conductivity at 20 °C are 0.598 W/m.°C and 0.237 W/m.°C, respectively. The glycerol thermal conductivity is 0.2837 W/m.°C, which is between them [30, 31]. Thus, the Corcione correlation, expressed in Equation (9), may predict the glycerol-based nanofluids. Consequently, the Corcione correlation was chosen for comparison in this investigation.

$$\frac{k_{eff}}{k_f} = 1 + 4.4 \, \text{Re}^{0.4} \, \text{Pr}^{0.66} \left(\frac{T}{T_{fr}}\right)^{10} \left(\frac{k_p}{k_f}\right)^{0.03} \phi^{0.66} \qquad (9)$$

where Re is the nanoparticle Reynolds number, Pr is the Prandtl number of the base fluid, T is the nanofluid temperature, T_{fr} is the freezing point of the base liquid in Kelvin, k_p is the nanoparticle thermal conductivity and ϕ is the volume fraction of the suspended nanoparticles.

Corcione derived the Reynolds number (Re) from the nanoparticle Brownian velocity (υ_B). The authors assumed no agglomeration to occur in the nanofluid. Corcione defined τ_D, expressed in Equation (10), as the time necessary for a nanoparticle of diameter d_p (nm) to cover the distance equal to its size in the base fluid of viscosity μ_f (kg/m.s), as proposed by Keblinski *et al.* [50].

$$\tau_D = \frac{d_p^2}{6D} = \frac{\pi \mu_f d_p^3}{2\kappa T} \qquad (10)$$

Where, T is the nanofluid temperature in K, D is the Einstein diffusion coefficient and κ is the Boltzmann's constant.

$$\upsilon_B = \frac{2\kappa T}{\pi \mu_f d_p^2} \tag{11}$$

$$\mathrm{Re} = \frac{2\rho_f \kappa T}{\pi \mu_f^2 d_p} \tag{12}$$

Comparison between theoretical and empirical models and experimental data

Figure 10 presents a comparison at room temperature between experimental data variation with volume fraction and those predicted by the Maxwell [48], Bruggeman [11], effective medium theory [18] models and the Corcione model [22] for thermal conductivity ratio for MgO-glycerol nanofluids. It is observed that the Corcione model shows an increase of k_{eff}/k_f with an increase in volume fraction and a decrease in particle size, but it underpredicts the measured experimental data. On the other hand, the Maxwell and Bruggeman effective medium theory models are unable to predict the correct thermal conductivity. These findings were also observed for the experiment's temperature range.

Figure 11 presents a comparison between experimental data variation with temperature and those predicted by the Maxwell [48], Bruggeman [11] and Effective medium theory [18] models and the Corcione model [22] for thermal conductivity ratio for 4% MgO-glycerol nanofluids. The Maxwell, Bruggeman and effective medium theory models did not show an explicit increase in the thermal conductivity ratio with temperature as the Corcione model did. None of these models

accurately predicted the experimentally determined values of the thermal conductivity ratio of MgO-glycerol-based nanofluids for all three sizes of MgO nanofluids.

Figure 12 shows the thermal conductivity ratio variation of 4% MgO nanofluids with nanoparticle diameter. The thermal conductivity ratio predicted by the Corcione model [22] decreases with an increase in nanoparticle size, but underpredicts the experimental data, as previously depicted in both the volume fraction and temperature variations. Similar observations are made for 0.5%, 1% and 2% MgO nanofluids. The Maxwell [48] and Bruggeman [11] and effective medium theory models [18] did not show an increase in the thermal conductivity ratio as diameters decreased. They underpredict the MgO-glycerol experimental data.

It is noticed that all of the models previously presented fail to predict the experimental data of MgO-glycerol nanofluids for all three sizes. They all underpredict the thermal conductivity ratio for MgO nanofluids of volume fractions ranging from 0.5% to 4%, measured in the temperature range of 20 °C to 45 °C. The classical models and Corcione equation could not explain the enhancement of the thermal conductivity of MgO-glycerol nanofluids. Each existing correlation model works for the particular nanofluid and conditions.

New empirical correlation for the thermal conductivity ratio of MgO-glycerol nanofluids

A new empirical correlation for thermal conductivity of MgO-glycerol nanofluids is determined. The novel equation is a modified version of a non-dimensional model proposed by Corcione [22]. The regression analysis is used to determine the relationship between the studied

parameters. The F-statistic and associated p-value are used to verify if the relationship between Y and Xj predictor variables is not random ($p < 0.05$). The t-statistic and related p-value assess the reliability of the partial regression coefficients ($p < 0.0\,5$) in the equation (9) [51]. In the proposed correlation of the thermal conductivity of MgO-glycerol nanofluid, the nanoparticle thermal conductivity is normalised with the thermal conductivity of base fluid (k_f). The nanoparticle diameter (d_p), nanofluid temperature and viscosity of the base fluids are normalised in the Reynolds number, as defined by Equation (13). The developed empirical correlation, which is expressed by Equation (13), is the result of the regression analysis with a 95% confidence level.

$$\frac{k_{eff}}{k_f} = 1 + \mathrm{Re}^{0.0603} \mathrm{Pr}^{0.1065} \phi^{0.9918} \left(\frac{k_p}{k_f}\right)^{0.3647} \tag{13}$$

with $\mathrm{Pr} = \dfrac{\mu_f\, c_{pf}}{k_f}$ \hfill (14)

Where Re is the nanoparticle Reynolds number, Pr is the Prandtl number of the base fluid (glycerol), ϕ is the nanoparticle volume fraction, C_{pf} is the specific heat of the base fluid, k_p is the thermal conductivity of the MgO nanoparticles (equal to 48.4 W/mK), k_f is the thermal conductivity of the glycerol (W/mK).

The new correlation of thermal conductivity of MgO-glycerol nanofluid is satisfactory for 20 ˚C $< T < 45$ ˚C, $0.5\% < \phi < 4\%$ and 21.1 nm $< d_p < 123.7$ nm. The range of Re (equation (12)) and Pr vary are from $1.12*10^{-11}$ to $2.91*10^{-9}$ and 2119 to 12798, respectively. Equation (13),

converging at 10^{-15}, has an adjusted $r^2 = 0.994$, $F = 9.99*10^5$ and significant p-value $= 0.0000$. The t-statistic of the exponents of Re, Pr, ϕ and k_p/k_f are 8.9, 6.4, 76.5 and 20.5 respectively. The p-values associated to the t-ratio of all their exponents and slope of the equation are equal to 0.0000 (p < 0.001). The statistical significance of all the exponents of the equation is high. In the general Corcione model [22], the p-value of the slope of the equation and the exponents of both Prandtl number and temperature were not statistically significant. There was high linear correlation (r $= 0.9992$) between the terms k_p/k_f and the slope of the equation, after removal of the temperature term (T/T_{fr}). Thus, the slope term was also removed to deal with the multicollinearity in the model. However, the temperature is still present in the new model, as the Reynolds number is directly proportional to temperature. There is no autocorrelation in the residuals and the residual sum is zero. The comparison between the predicted thermal conductivity ratio from the present model and the experimental results shows an excellent agreement with maximum relative error of $+ 1.15\%$, -0.58% and the average relative error of - 0.04% (see Figure 13). The present analysis provides evidence that the novel model is statistically significant.

Figure 14 shows an intense temperature dependence of the Reynolds number for 21.1 nm in comparison to both 103.8 nm and 123.7 nm MgO nanofluids. The Reynolds number increases as nanoparticle size decreases, because the Brownian velocity effect is much stronger for smaller particles than for bigger particles (Figure 15). For a given temperature and volume fraction, the TCR decreases as the nanoparticle size increases.

Figure 16 depicts the impact of temperature on the three standardised parameters of the novel equation for 21.1 nm MgO-glycerol nanofluid at 1% volume fraction. The three standardised

parameters are the Reynolds number term $(Re)^{0.0603}$, Prandtl number term $(Pr)^{0.1065}$ and thermal conductivity of nanoparticle normalised to the thermal conductivity of glycerol term $[k_p/k_f]^{0.3647}$.

Figure 16 discloses that the normalised Re increases with a rise in temperature, whereas the standardised Pr decreases. The magnitude of variation, in absolute value, of standardised Re is bigger than standardised Pr. The combined effect of normalised Re and Pr slightly increases with temperature rise. However, the impact of both standardised Re and Pr numbers on the k_{eff}/k_f are small compared to the standardised k_p/k_f. The normalised term (k_p/k_f) at 20 ˚C is 27 and 30 times bigger than the effect of standardised (Re) term for the 21.1 nm and both 104 nm and 119 nm MgO-glycerol nanofluids respectively (see Figure 16). The normalised k_p/k_f is the major parameter describing the enhancement of the TCR of MgO-glycerol nanofluids, as opposed to the Reynolds number for the case of Al_2O_3 water nanofluids [52]. This can be explained by the very low Brownian velocity occurring in the glycerol base fluid (see Figure 15) due to its very high viscosity (about 1 530 bigger than water at 20 ˚C) and capacity to diffuse heat, which is very low compared to its momentum, as opposed to water [53]. The described phenomenon strengthens with the increased concentration of suspended MgO nanoparticles in the glycerol. Altogether, the model depicts that the thermal conductivity ratio increases with an increase in volume fraction, decreases with an increase in nanoparticle size and is unaffected with temperature rise.

Conclusions

In this study, the thermal conductivity ratio of MgO-glycerol nanofluids is investigated experimentally. The influence of volume fractions ranging from 0.5% to 4%, temperatures between 20 °C and 45 °C and particle sizes of 21.1 nm, 103.8 nm and 123.7 nm on the thermal conductivity were presented and discussed. The following conclusions are drawn from the results:

1. The experimental results demonstrate that using MgO-glycerol nanofluids enhances the effective thermal conductivity of the base fluid (glycerol). However, the effective thermal conductivity of the nanofluid has the same trend as the base fluid (glycerol) pattern, but on another level of magnitude.

2. The thermal conductivity ratio increases linearly with volume fraction of MgO nanoparticles at a constant temperature and displays a maximum enhancement of $\approx 19\%$ at 4% volume fraction of MgO-glycerol. The k_{eff}/k_f is unaffected with temperature variation.

3. The inverse dependence of the diameter on the effective thermal conductivity ratio is observed with the nanoparticle size variation.

4. The MgO-glycerol nanofluids are stable for at least 48 hours after preparation without any surfactants.

5. The possible models for glycerol-based nanofluids fail to accurately predict the thermal conductivity of MgO-glycerol nanofluids. Therefore, a new empirical correlation has been developed.

Acknowledgements

Nomenclature

A	Projected area of nanoparticle, m^2
$circ$	Circularity
c_p	Specific heat, J/kg.K
d	Diameter, nm
D	Einstein diffusion coefficient
F	F-statistic
hkl	Miller indices
k	Thermal conductivity (W/mK)
K	A shape factor
p-value	probability of the results is extreme or more extreme than the null hypothesis
P	Outline perimeter of nanoparticle, m
Pr	Prandtl number

r	Pearson correlation coefficient
r^2	Proportion of variation of Y explained by X
Re	Reynolds number
SD	Standard deviation
SSA	Specific surface area, m^2
T	Temperature, ˚C
u	Uncertainty
v	Brownian velocity, µm/s
W	Weight, kg

Greek symbols

β	Full-width at half maximum, rad
Θ	Diffraction angle, rad
κ	Boltzmann's constant, J/K
λ	X-ray wavelength, Å
μ	Viscosity, N.s/m^2
ρ	Density, kg/m^3
τ_D	Time necessary for nanoparticle of diameter d_p to cover the distance equal to its

size, s

ϕ	Volume fraction

Subscripts

B	Brownian
crist	Crystallite
eff	Effective
f	Fluid
fr	Freezing point of the base liquid
k	Thermal conductivity
p	Particle

Abbreviations

ASTM	American Society for Testing and Materials
EG	Ethylene glycol
FWHM	Full width at half maximum
MgO	Magnesium oxide
PDF	Powder Diffraction File
S	Sample
TCR	Thermal conductivity ratio
TEM	Transmission electron microscopy
XRD	X-ray powder diffraction
XRF	X-ray fluorescence spectroscopy

References

[1] Choi, S., Enhancing thermal conductivity of fluids with nanoparticles, *Developments and Applications of Non-Newtonian Flows*, New York, FED-Vol. 231/MD-Vol. 66, ASME, pp 99-105, 1995.

[2] Nazari, M., Karami, M., and Ashouri, M., Comparing the thermal performance of water, Ethylene Glycol, Alumina and CNT nanofluids in CPU cooling: Experimental study, *Experimental Thermal and Fluid Science*, vol. 57, pp. 371-377, 2014.

[3] Ghanbarpour, M., Bitaraf Haghigi, E., and Khodabandeh, R., Thermal properties and rheological behavior of water based Al_2O_3 nanofluid as a heat transfer fluid, *Experimental Thermal and Fluid Science*, vol. 53, pp. 227-235, 2014.

[4] Saleh, R., Putra, N., Wibowo, R. E., Septiadi, W. N., and Prakoso, S. P., Titanium dioxide nanofluids for heat transfer applications, *Experimental Thermal and Fluid Science*, vol. 52, pp. 19-29, 2014.

[5] Jamal-Abad, M. T., Zamzamian, A., and Dehghan, M., Experimental studies on the heat transfer and pressure drop characteristics of Cu–water and Al–water nanofluids in a spiral coil, *Experimental Thermal and Fluid Science*, vol. 47, pp. 206-212, 2013.

[6] Özerinç, S., Kakaç, S., and YazIcIoğlu, A. G., Enhanced thermal conductivity of nanofluids: A state-of-the-art review, *Microfluidics and Nanofluidics*, vol. 8, no. 2, pp. 145-170, 2010.

[7] Mallick, S. S., Mishra, A., and Kundan, L., An investigation into modelling thermal conductivity for alumina–water nanofluids, *Powder Technology*, vol. 233, pp. 234-244, 2013.

[8] Duangthongsuk, W., and Wongwises, S., Measurement of temperature-dependent thermal conductivity and viscosity of TiO$_2$-water nanofluids, *Experimental Thermal and Fluid Science*, vol. 33, no. 4, pp. 706-714, 2009.

[9] Feng, Y., Yu, B., Xu, P., and Zou, M., 2007, The effective thermal conductivity of nanofluids based on the nanolayer and the aggregation of nanoparticles, *Journal of Physics D: Applied Physics*, vol. 40, no. 10, pp. 3164-3171, 2007.

[10] Prasher, R., Bhattacharya, P., and Phelan, P. E., Brownian-Motion-Based Convective-Conductive Model for the Effective Thermal Conductivity of Nanofluids, *Journal of Heat Transfer*, vol. 128, no. 6, pp. 588-595, 2006.

[11] Wang, X.-Q., and Mujumdar, A. S., Heat transfer characteristics of nanofluids: a review, *International Journal of Thermal Sciences*, vol. 46, no. 1, pp. 1-19, 2007.

[12] Wang, B.-X., Zhou, L.-P., and Peng, X.-F., A fractal model for predicting the effective thermal conductivity of liquid with suspension of nanoparticles, *International Journal of Heat and Mass Transfer*, vol. 46, no. 14, pp. 2665-2672, 2003.

[13] Vajjha, R. S., and Das, D. K., Experimental determination of thermal conductivity of three nanofluids and development of new correlations, *International Journal of Heat and Mass Transfer*, vol. 52, no. 21-22, pp. 4675-4682, 2009.

[14] Khanafer, K., and Vafai, K., A critical synthesis of thermophysical characteristics of nanofluids, *International Journal of Heat and Mass Transfer*, vol. 54, no. 19-20, pp. 4410-4428, 2011.

[15] Xie, H., Fujii, M., and Zhang, X., Effect of interfacial nanolayer on the effective thermal conductivity of nanoparticle-fluid mixture, *International Journal of Heat and Mass Transfer*, vol. 48, no. 14, pp. 2926-2932, 2005.

[16] Xue, Q., and Xu, W.-M., A model of thermal conductivity of nanofluids with interfacial shells, *Materials Chemistry and Physics*, vol. 90, no. 2–3, pp. 298-301, 2005.

[17] Choi, S. U. S., Zhang, Z. G., Yu, W., Lockwood, F. E., and Grulke, E. A., Anomalous thermal conductivity enhancement in nanotube suspensions, *Applied Physics Letters*, vol. 79, no. 14, pp. 2252-2254, 2001.

[18] Timofeeva, E., Gavrilov, A., McCloskey, J., Tolmachev, Y., Sprunt, S., Lopatina, L., and Selinger, J., Thermal conductivity and particle agglomeration in alumina nanofluids: Experiment and theory, *Physical Review E*, vol. 76, no. 0612301, pp. 1-16, 2007.

[19] Kole, M., and Dey, T. K., Effect of prolonged ultrasonication on the thermal conductivity of ZnO–ethylene glycol nanofluids, *Thermochimica Acta*, vol. 535, pp. 58-65, 2012.

[20] Mahbubul, I. M., Fadhilah, S. A., Saidur, R., Leong, K. Y., and Amalina, M. A., Thermophysical properties and heat transfer performance of Al_2O_3/R-134a nanorefrigerants, *International Journal of Heat and Mass Transfer*, vol. 57, no. 1, pp. 100-108, 2013.

[21] Xie, H., Yu, W., and Chen, W., MgO nanofluids: higher thermal conductivity and lower viscosity among ethylene glycol-based nanofluids containing oxide nanoparticles, *Journal of Experimental Nanoscience*, vol. 5, no. 5, pp. 463-472, 2010.

[22] Corcione, M., Empirical correlating equations for predicting the effective thermal conductivity and dynamic viscosity of nanofluids, *Energy Conversion and Management*, vol. 52, no. 1, pp. 789-793, 2011.

[23] ASTM, Proposed ASTM Engine Coolant Standards Focus on Glycerin, ASTM International, 2010. Available: http://www.astmnewsroom.org/default.aspx?pageid=2115 . [Online; accessed 14 April 2014].

 [24] SDA, Glycerine—An Overview, The Soap and Detergent Association, Glycerine and Oleochemical Division, New York, 1990. Available: www.aciscience.org/docs/glycerine_-_an_overview.pdf. [Online; accessed 14 April 2014].

[25] Materials, N. A., Nanoparticles: Magnesium Oxide (MgO, 99%, 100 nm), Nanostructured and Amorphous Materials, 2014. Available: http://www.nanoamor.com/nanoscale_elements__oxides__carbides___nitrides. [Online; accessed 14 April 2014].

[26] Nanomaterials, U. R., Nanopowder: Single-Element Oxides (MgO, 99+%, 20 nm), US Research Nanomaterials, 2014. Available: http://www.us-nano.com/nanopowders. [Online; accessed 14 April 2014].

[27] Jeol, S. I., JEM-2100F Transmission Electron Microscope, 2015. Available: http://www.jeolusa.com/PRODUCTS/TransmissionElectronMicroscopes%28TEM%29/200kV/JEM-2100F/tabid/208/Default.aspx. [Online; accessed 6 March 2015].

[28] Devices, D., KD2 Pro thermal properties analyzer: operator's manual version 4, Decagon Devices, Pullman, WA, 5 May 2015. Available: http://www.decagon.com/education/kd2-pro-manual/. [Online; accessed 6 June 2015].

 [29] Salman, B. H., Mohammed, H. A., Munisamy, K. M., and Kherbeet, A. S., Characteristics of heat transfer and fluid flow in microtube and microchannel using conventional fluids and nanofluids: A review, *Renewable and Sustainable Energy Reviews*, vol. 28, pp. 848-880, 2013.

[30] Hielscher, U. T., UP200H / UP200S – Ultrasonic Power for the Lab, 2014. Available: http://www.hielscher.com/200s_p.htm . [Online; accessed 14 April 2014].

[31] Tshimanga, N., Sharifpur, M., and Meyer, J., The effect of sonication time on effective thermal conductivity of Glycerol-MgO based nanofluids, *Proc. Proceedings of the 15th International Heat Transfer Conference*, Kyoto, Japan, IHTC15-8595, pp. 11-15, 2014.

[32] Hewitt, G. F., *Heat Exchanger Design Handbook 2008: Physical properties, Part 5,* pp. 5.5.10-71 , Begell house, New York, USA, 2008.

[33] Incropera, F. P., and DeWitt, D. P., *Introduction to Heat Transfer*, pp. 830-844, John Wiley & Sons, New York, USA, 1996.

[34] Suryanarayana, C., and Norton, M. G., *X-ray Diffraction: A Practical Approach*, Plenum Publishing Corporation, pp. 207-271, New York, USA, 1998.

[35] Speakman, S. A., *Estimating Crystallite Size Using XRD*, pp. 1-93, MIT Center for Materials Science and Engineering, Cambridge, USA, 2012.

[36] Baecker, V., *Workshop: Image processing and analysis with ImageJ and MRI Cell Image Analyzer*, Montpellier RIO Imaging, pp. 1-93, Languedoc-Roussillon, France, 2010.

[37] Halelfadl, S., Maré, T., and Estellé, P., Efficiency of carbon nanotubes water based nanofluids as coolants, *Experimental Thermal and Fluid Science*, vol. 53, pp. 104-110, 2014.

[38] Khedkar, R. S., Sonawane, S. S., and Wasewar, K. L., Influence of CuO nanoparticles in enhancing the thermal conductivity of water and monoethylene glycol based nanofluids, *International Communications in Heat and Mass Transfer*, vol. 39, no. 5, pp. 665-669, 2012.

[39] Xuan, Y., Heat transfer enhancement of nanofuids, *International Journal of Heat and Fluid Flow*, vol. 21, pp. 58-64, 2000.

[40] Kole, M., and Dey, T. K., Thermophysical and pool boiling characteristics of ZnO-ethylene glycol nanofluids, *International Journal of Thermal Sciences*, vol. 62, pp. 61-70, 2012.

[41] Xie, H., Yu, W., Li, Y., and Chen, L., Discussion on the thermal conductivity enhancement of nanofluids, *Nanoscale Research Letters*, vol. 6, no. 124, pp. 1-12, 2011.

[42] Suganthi, K. S., and Rajan, K. S., Temperature induced changes in ZnO–water nanofluid: zeta potential, size distribution and viscosity profiles, *International Journal of Heat and Mass Transfer*, vol. 55, no. 25, pp. 7969-7980, 2012.

[43] Murshed, S. M. S., Leong, K. C., and Yang, C., Investigations of thermal conductivity and viscosity of nanofluids, *International Journal of Thermal Sciences*, vol. 47, no. 5, pp. 560-568, 2008.

[44] Liu, M.-S., Lin, M. C.-C., Tsai, C. Y., and Wang, C.-C., Enhancement of thermal conductivity with Cu for nanofluids using chemical reduction method, *International Journal of Heat and Mass Transfer*, vol. 49, no. 17–18, pp. 3028-3033, 2006.

[45] Hong, K. S., Hong, T.-K., and Yang, H.-S., Thermal conductivity of Fe nanofluids depending on the cluster size of nanoparticles, *Applied Physics Letters*, vol. 88, no. 031901, pp. 1-3, 2006.

[46] Sharifpur, M., Ntumba, T., and Meyer, J. P., Parametric analysis of effective thermal conductivity models for nanofluids, *Proc. ASME 2012 International Mechanical Engineering Congress and Exposition*, Houston, USA, paper IMECE2012-85093, pp. 1-11, 2012.

[47] Aybar, H. Ş., Sharifpur, M., Azizian, M. R., Mehrabi, M., and Meyer, J. P., A Review of Thermal Conductivity Models for Nanofluids, *Heat Transfer Engineering*, vol. 36, no. 13, pp. 1085-1110, 2014.

[48] Buongiorno, J., Venerus, D. C., Prabhat, N., McKrell, T., Townsend, J., Christianson, R., Tolmachev, Y. V., Keblinski, P., Hu, L.-w., Alvarado, J. L., Bang, I. C., Bishnoi, S. W., Bonetti, M., Botz, F., Cecere, A., Chang, Y., Chen, G., Chen, H., Chung, S. J., Chyu, M. K., Das, S. K., Di Paola, R., Ding, Y., Dubois, F., Dzido, G., Eapen, J., Escher, W., Funfschilling, D., Galand, Q., Gao, J., Gharagozloo, P. E., Goodson, K. E., Gutierrez, J. G., Hong, H., Horton, M., Hwang, K. S., Iorio, C. S., Jang, S. P., Jarzebski, A. B., Jiang, Y., Jin, L., Kabelac, S., Kamath, A., Kedzierski, M. A., Kieng, L. G., Kim, C., Kim, J.-H., Kim, S., Lee, S. H., Leong, K. C., Manna, I., Michel, B., Ni, R., Patel, H. E., Philip, J., Poulikakos, D., Reynaud, C., Savino, R., Singh, P. K., Song, P., Sundararajan, T., Timofeeva, E., Tritcak, T., Turanov, A. N., Van Vaerenbergh, S., Wen, D., Witharana, S., Yang, C., Yeh, W.-H., Zhao, X.-Z., and Zhou, S.-Q., A benchmark

study on the thermal conductivity of nanofluids, *Journal of Applied Physics*, vol. 106, no. 094312, pp. 1-14, 2009.

[49] Yu, W., and Choi, S., The role of interfacial layers in the enhanced thermal conductivity of nanofluids: a renovated Maxwell model, *Journal of Nanoparticle Research*, vol. 5, no. 1-2, pp. 167-171, 2003.

[50] Keblinski, P., Phillpot, S. R., Choi, S. U. S., and Eastman, J. A., Mechanisms of heat flow in suspensions of nano-sized particles (nanofluids), *International Journal of Heat and Mass Transfer*, vol. 45, no. 4, pp. 855-863, 2002.

[51] Kleinbaum, D. G., Kupper, L. L., Nizam, A., and Muller, K. E., *Applied regression analysis and other multivariable methods*, 4th ed., pp. 305-348, Thomson Higher Education, Belmont, USA, 2008.

[52] Chon, C. H., Kihm, K. D., Lee, S. P., and Choi, S. U. S., Empirical correlation finding the role of temperature and particle size for nanofluid (Al_2O_3) thermal conductivity enhancement, *Applied Physics Letters*, vol. 87, no. 153107, pp. 1-3, 2005.

[53] Cengel, Y. A., *Heat and Mass Transfer: A Practical Approach*, pp. 380-381, Mc Graw Hill, New York, USA, 2006.

Table 1: Properties of magnesium oxide

Diameter (nm)	Purity (%)	Morphology	SSA (m²/g)	True density (g/cm³) at 20 °C	Thermal conductivity (W/mK) [21]
20	99+	polyhedral	>60	3.58	48.4
40	99+	polyhedral	≈25	3.58	48.4
100	99+	polyhedral		3.58	48.4

Table 2: Chemical compositions of the MgO nanoparticles

Diameter (nm)	MgO	TiO$_2$	Fe$_2$O$_3$	CaO	Cr$_2$O$_3$	NiO	SO$_3$	LOI*
100	98.14	0.14	0.05	0.43	0.02	0.02	0.13	1.06
40	96.36	< 0.01	0.05	< 0.01	< 0.01	0.02	< 0.01	3.57
20	87.70	0.07	0.13	0.15	< 0.01	0.03	0.07	11.84

*LOI: Loss of Ignition

Table 3: Mineralogical composition of MgO nanoparticles

Mineral	Nanoparticles					
	20 nm MgO		40 nm MgO		100 nm MgO	
	Weight (%)	3 *SD*	Weight (%)	3 *SD*	Weight (%)	3 *SD*
Brucite (Mg(OH)$_2$	14.28	0.81	6.53	0.33	0.00	0
Periclase (MgO)	85.72	0.81	93.47	0.33	100.00	0

Table 4: TEM and crystalline sizes from XRD patterns sizes of MgO nanoparticles powders

Sample	Miller indices, hkl	d-spacing (Å)	$2\theta(°)$	FWHM (°Å)	Crystalline size (Å)	TEM particles size (nm)	SD of TEM size (nm)
S1	200	2.10800	50.24	0.57	20	21.1	4.1
	220	1.49058	73.79	0.7	18		
S2	200	2.10800	50.28	0.23	49	123.7	45.5
	220	1.49058	73.84	0.31	41		
S3	200	2.10647	50.26	0.24	48	103.8	28.1
	220	1.48948	73.82	0.31	41		

List of figures

Figure 1: Validation of experimental data

Figure 2: TEM image of MgO nanoparticles (a) 20 nm, (b) 40 nm and (c) 100 nm

Figure 3: Diameter distribution of MgO nanoparticles: (a) 20 nm, (b) 40 nm and (c) 100 nm
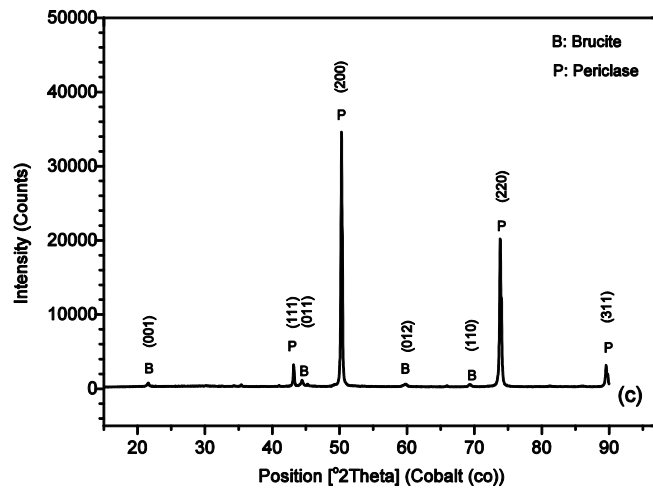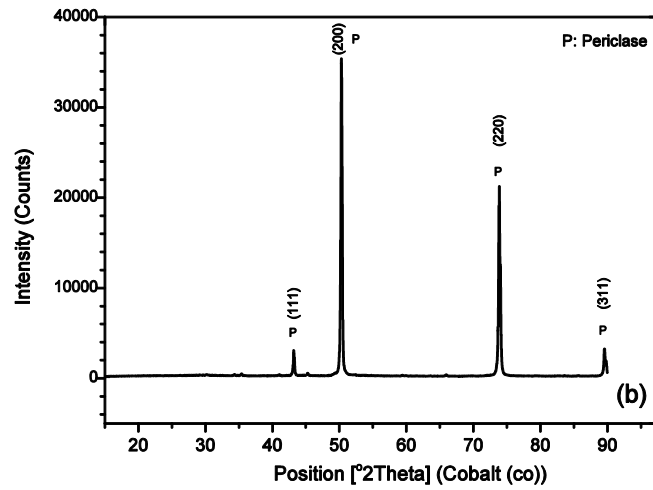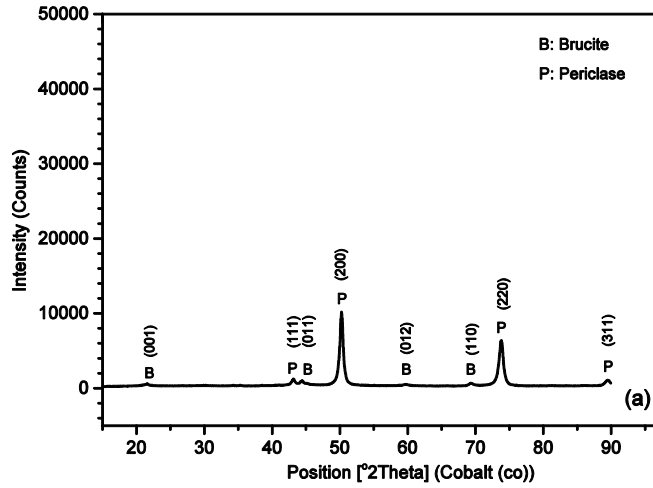
Figure 4: X-ray diffraction pattern of the MgO nanoparticles: (a) 21.1 nm, (b) 103.8 nm and (c) 123.7 nm powder
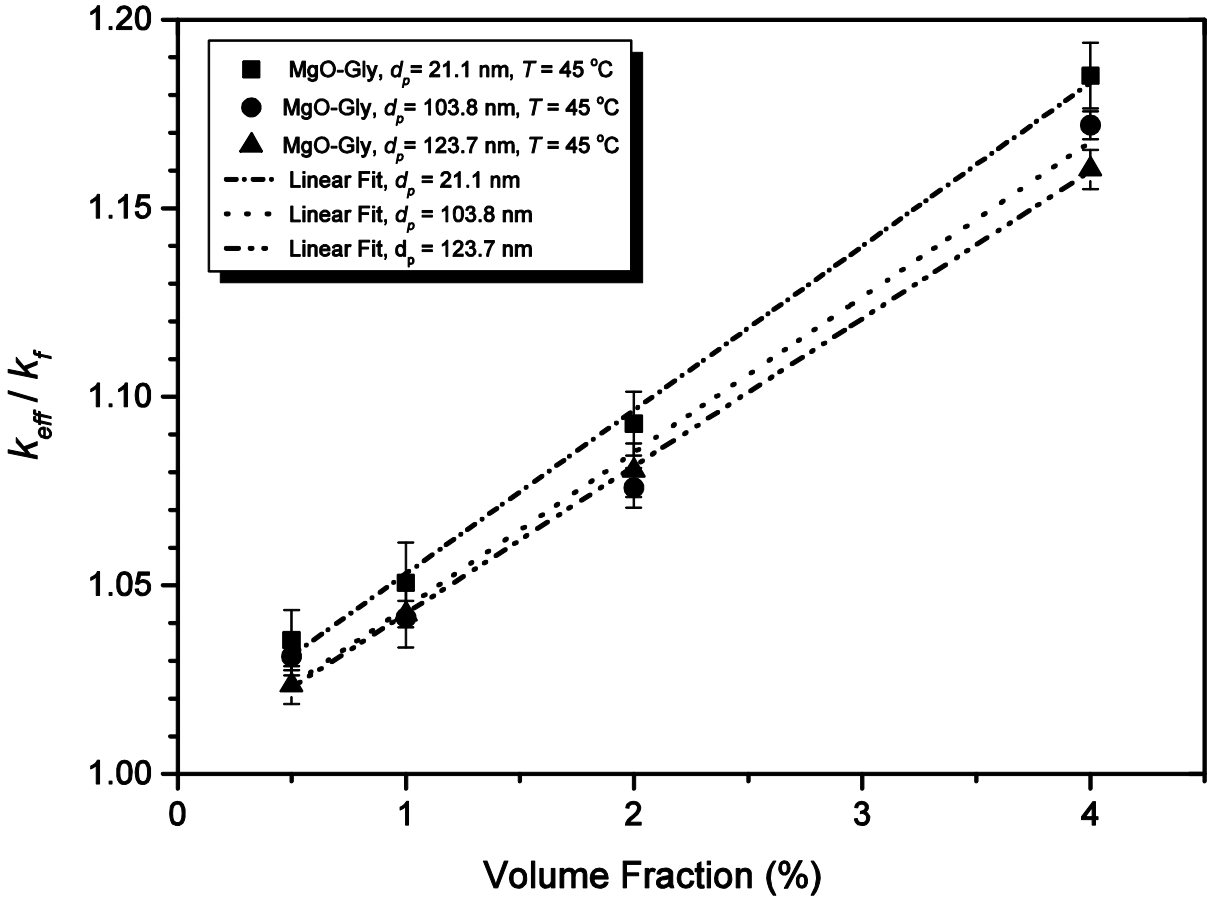
Figure 5: Influence of the nanoparticle volume fraction on the thermal conductivity ratio of the three set of MgO-glycerol nanofluids at 45 °C. Errors bars indicate standard deviation
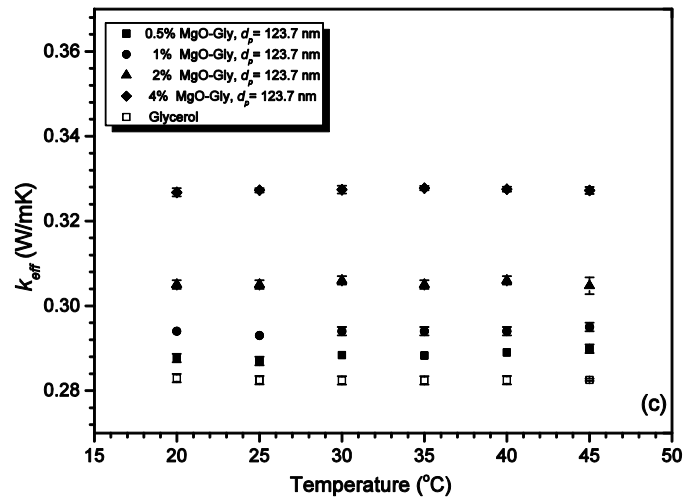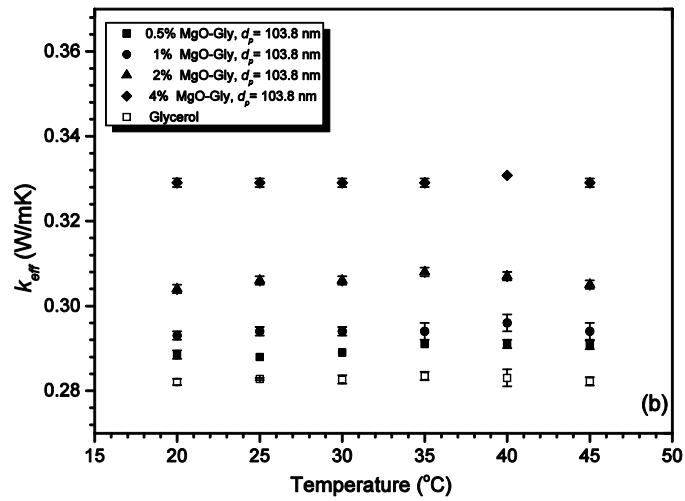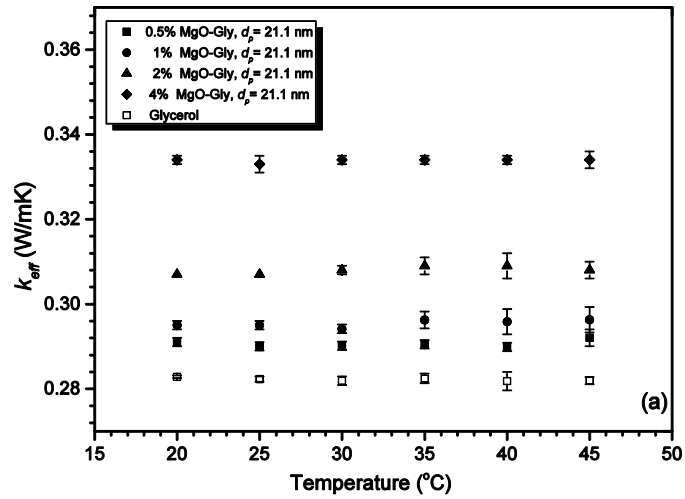
Figure 6: Temperature dependence of effective thermal conductivity of MgO-glycerol nanofluids at different MgO volume concentrations: (a) 21.1 nm, (b) 103.8 nm and (c) 123.7 nm
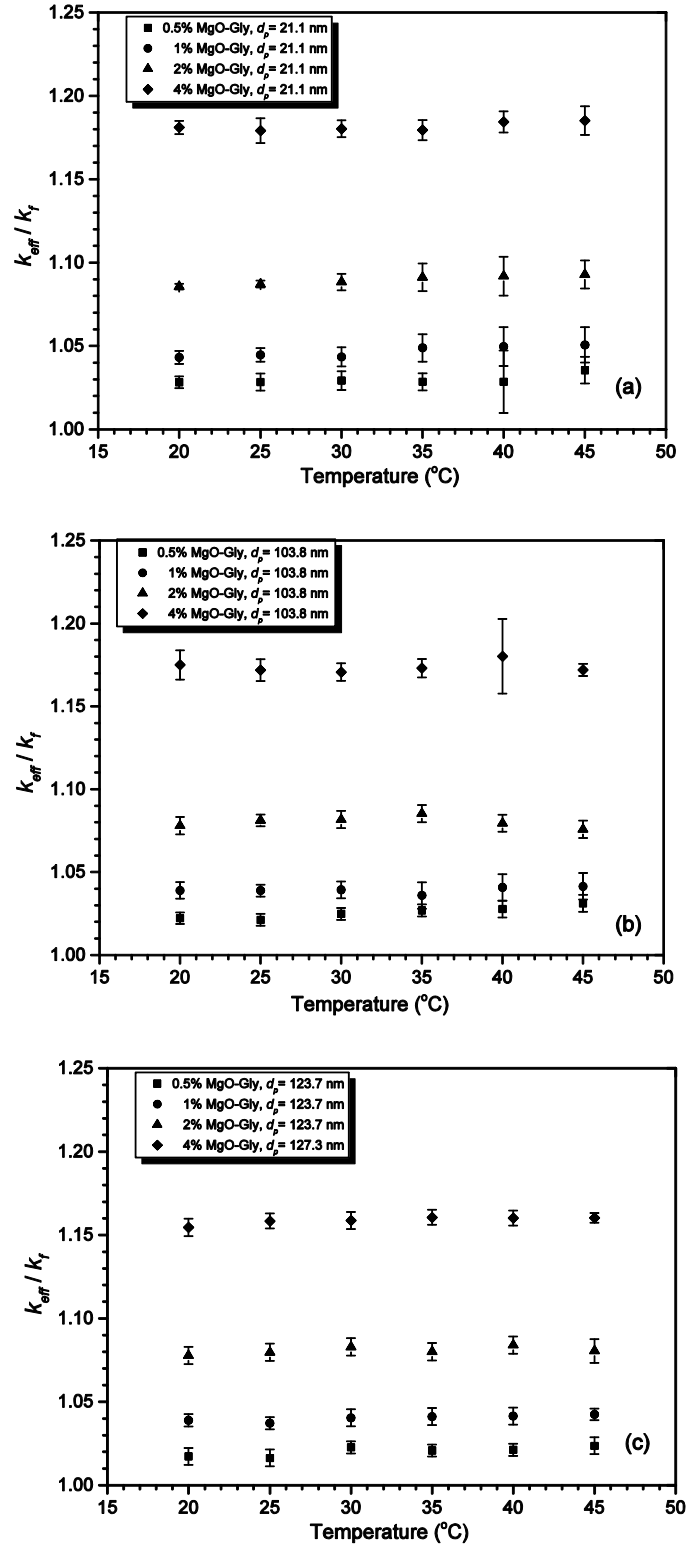
Figure 7: Temperature dependence of effective thermal conductivity ratio of MgO-glycerol nanofluids at different MgO volume concentrations: (a) 21.1 nm, (b) 103.8nm and (c) 123.7nm
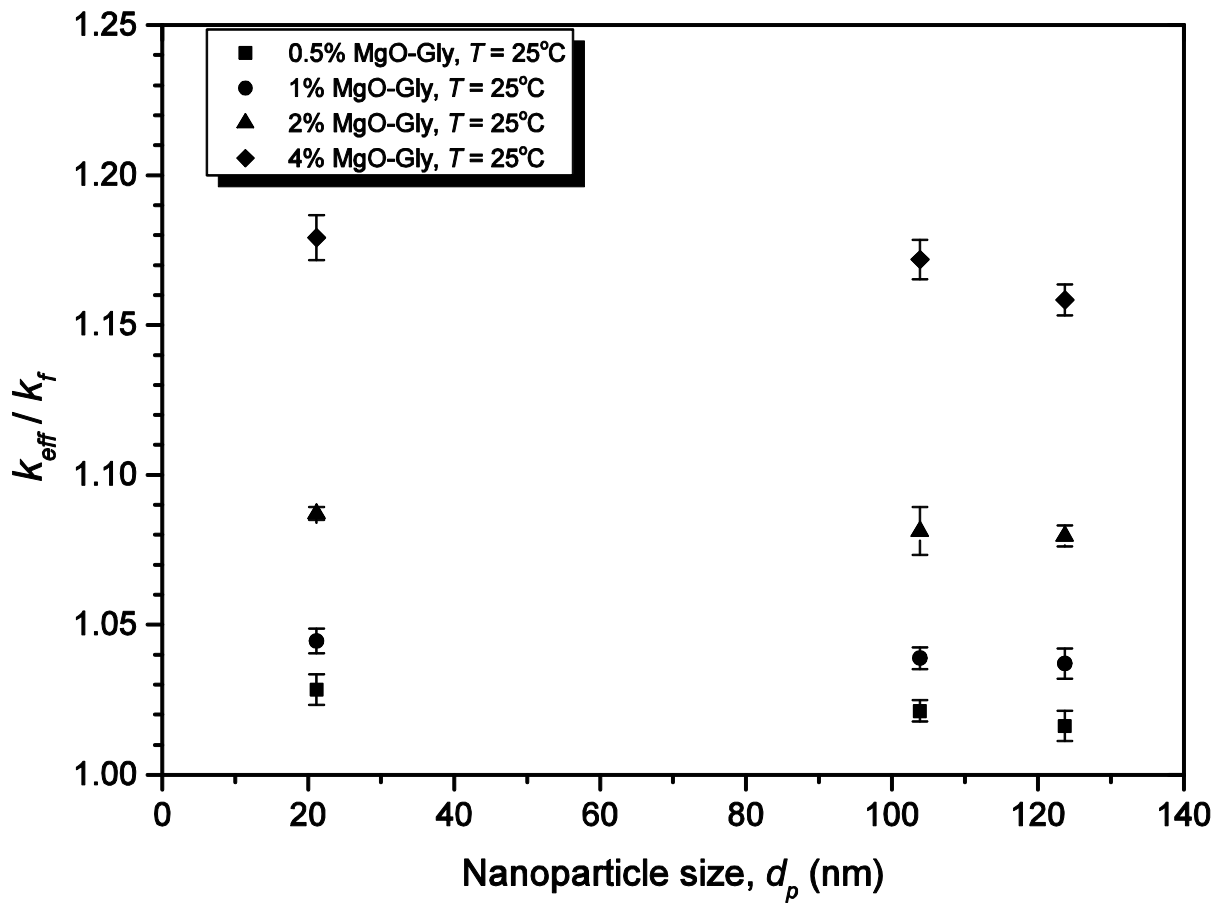
Figure 8: Influence of nanoparticle size on effective thermal conductivity ratio at three different volume fractions of MgO-glycerol nanofluid at 25 °C
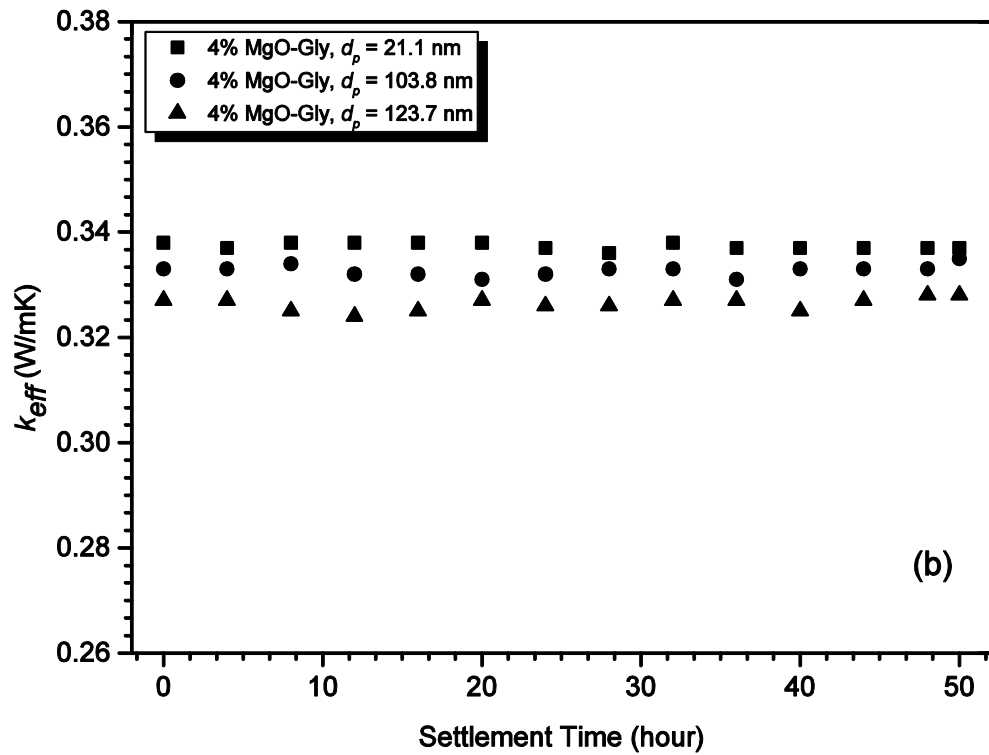
Figure 9: Influence of settlement time on the effective thermal conductivity of MgO-glycerol nanofluids: (a) 0.5% and (b) 4%

Figure 10: Comparison of thermal conductivity ratio variation with volume fraction of experimental data and existing equations for MgO-glycerol nanofluids at 25 ˚C

Figure 11: Comparison of thermal conductivity ratio variation with temperature between experimental data and existing equations for 4% MgO-glycerol nanofluids: (a) 21.1 nm, (b) 103.8 nm and (c) 123.7 nm

Figure 12: Comparison of thermal conductivity ratio variation with nanoparticle diameter between experimental data and existing equations for 4% MgO-glycerol nanofluids at 35 ˚C

Figure 13: Comparison of the thermal conductivity ratio between the predicted values from the present correlation and the experiments data on MgO-glycerol nanofluids
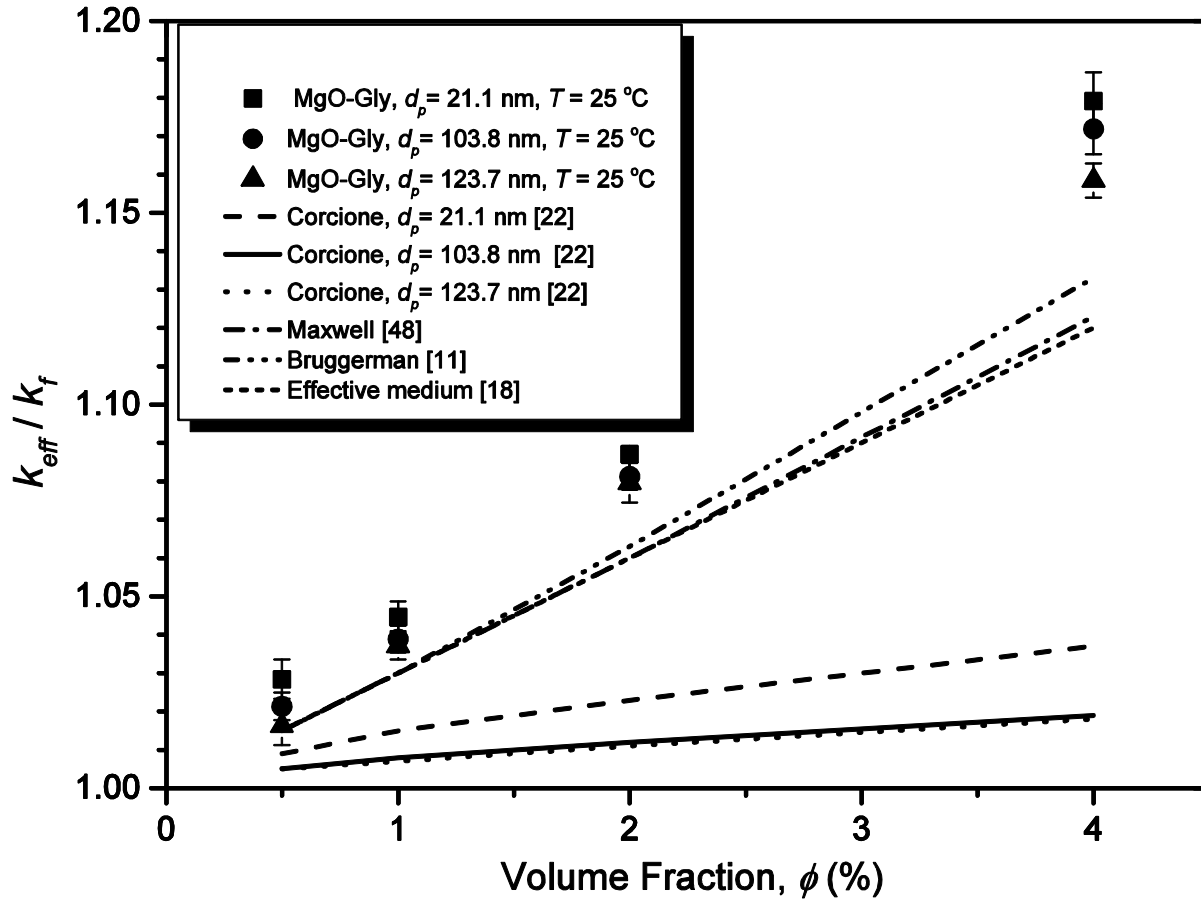
Figure 14: Reynolds number of different particle sizes of MgO-glycerol nanofluids

Figure 15: Brownian velocity of different particle sizes of MgO-glycerol nanofluids

Figure 16: Temperature dependence of the normalised effects of the three parameters of the novel correlation of the MgO-glycerol nanofluids

Figure 1: Validation of experimental data
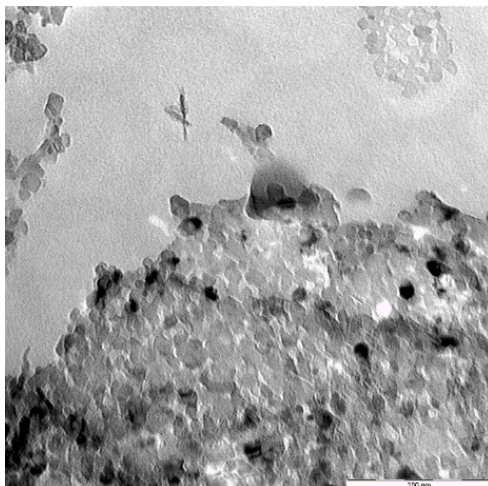
(a)
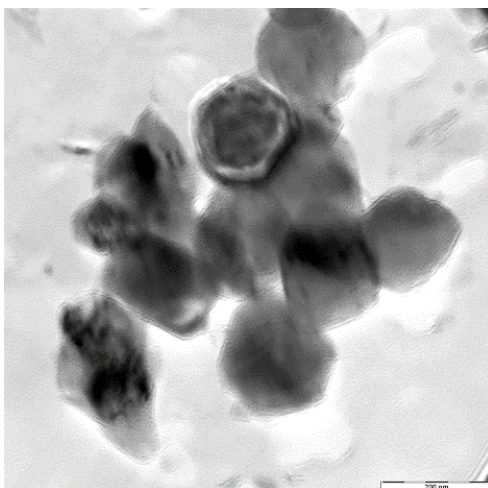
(b)
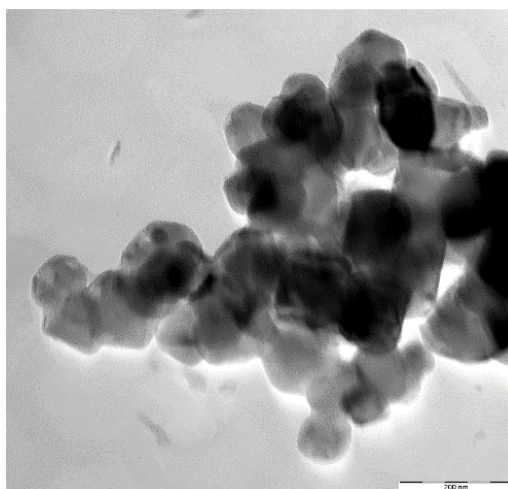
(c)

Figure 2: TEM image of MgO nanoparticles (a) 20 nm, (b) 40 nm and (c) 100 nm
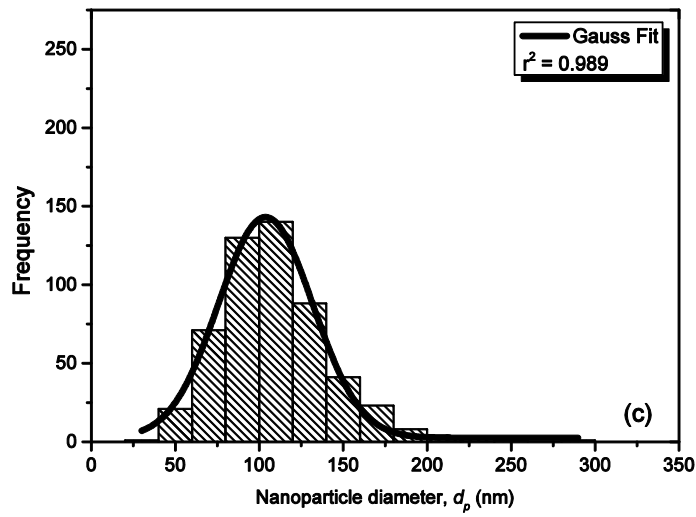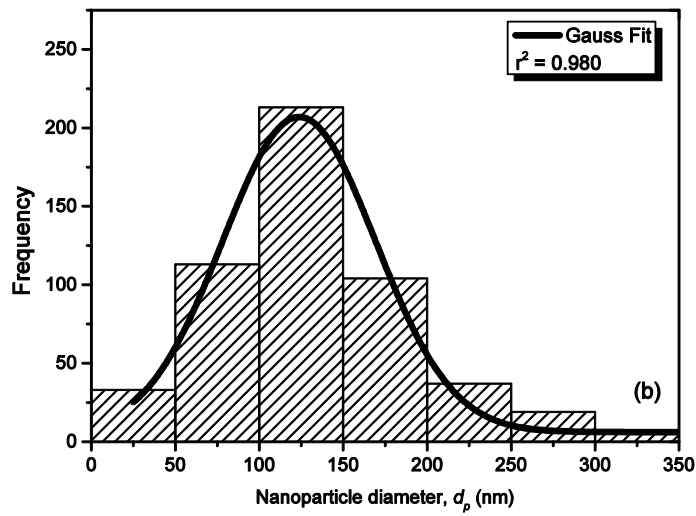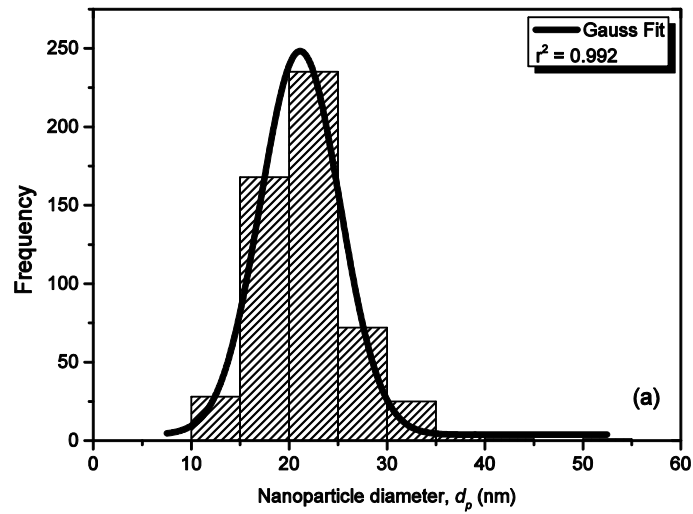
Figure 3: Diameter distribution of MgO nanoparticles: (a) 20 nm, (b) 40 nm and (c) 100 nm

Figure 4: X-ray diffraction pattern of the MgO nanoparticles: (a) 21.1 nm, (b) 103.8 nm and (c) 123.7 nm powder

Figure 5: Influence of the nanoparticle volume fraction on the thermal conductivity ratio of the three set of MgO-glycerol nanofluids at 45 °C. Error bars indicate standard deviation

Figure 6: Temperature dependence of effective thermal conductivity of MgO-glycerol nanofluids at different MgO volume concentrations: (a) 21.1 nm, (b) 103.8 nm and (c) 123.7 nm

Figure 7: Temperature dependence of effective thermal conductivity ratio of MgO-glycerol nanofluids at different MgO volume concentrations: (a) 21.1 nm, (b) 103.8nm and (c) 123.7nm

Figure 8: Influence of nanoparticle size on effective thermal conductivity ratio at three different volume fractions of MgO-glycerol nanofluid at 25 °C

Figure 9: Influence of settlement time on the effective thermal conductivity of MgO-glycerol nanofluids: (a) 0.5% and (b) 4%

Figure 10: Comparison of thermal conductivity ratio variation with volume fraction of experimental data and existing equations for MgO-glycerol nanofluids at 25 °C
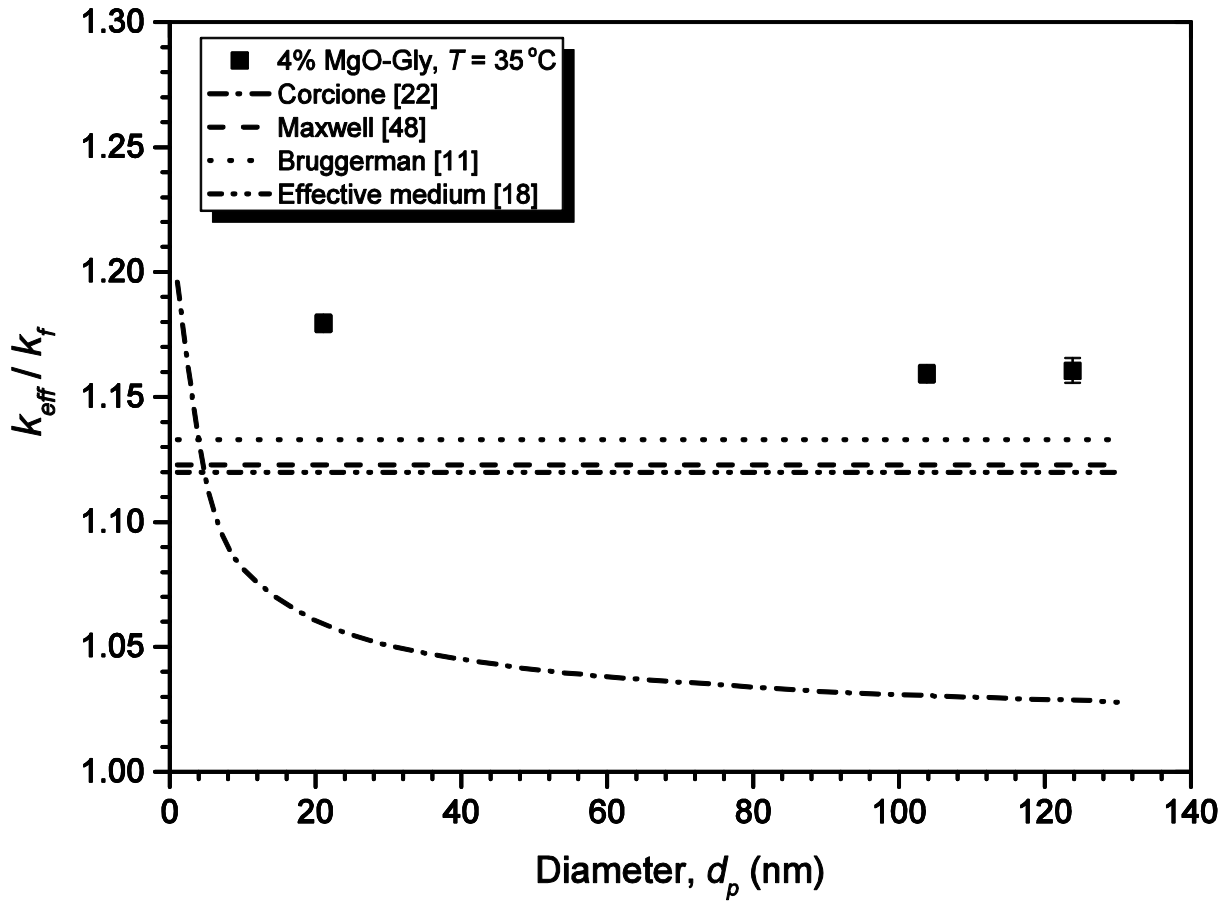
Figure 11: Comparison of thermal conductivity ratio variation with temperature between experimental data and existing equations for 4% MgO-glycerol nanofluids: (a) 21.1 nm, (b) 103.8 nm and (c) 123.7 nm

Figure 12: Comparison of thermal conductivity ratio variation with nanoparticle diameter between experimental data and existing equations for 4% MgO-glycerol nanofluids at 35 °C
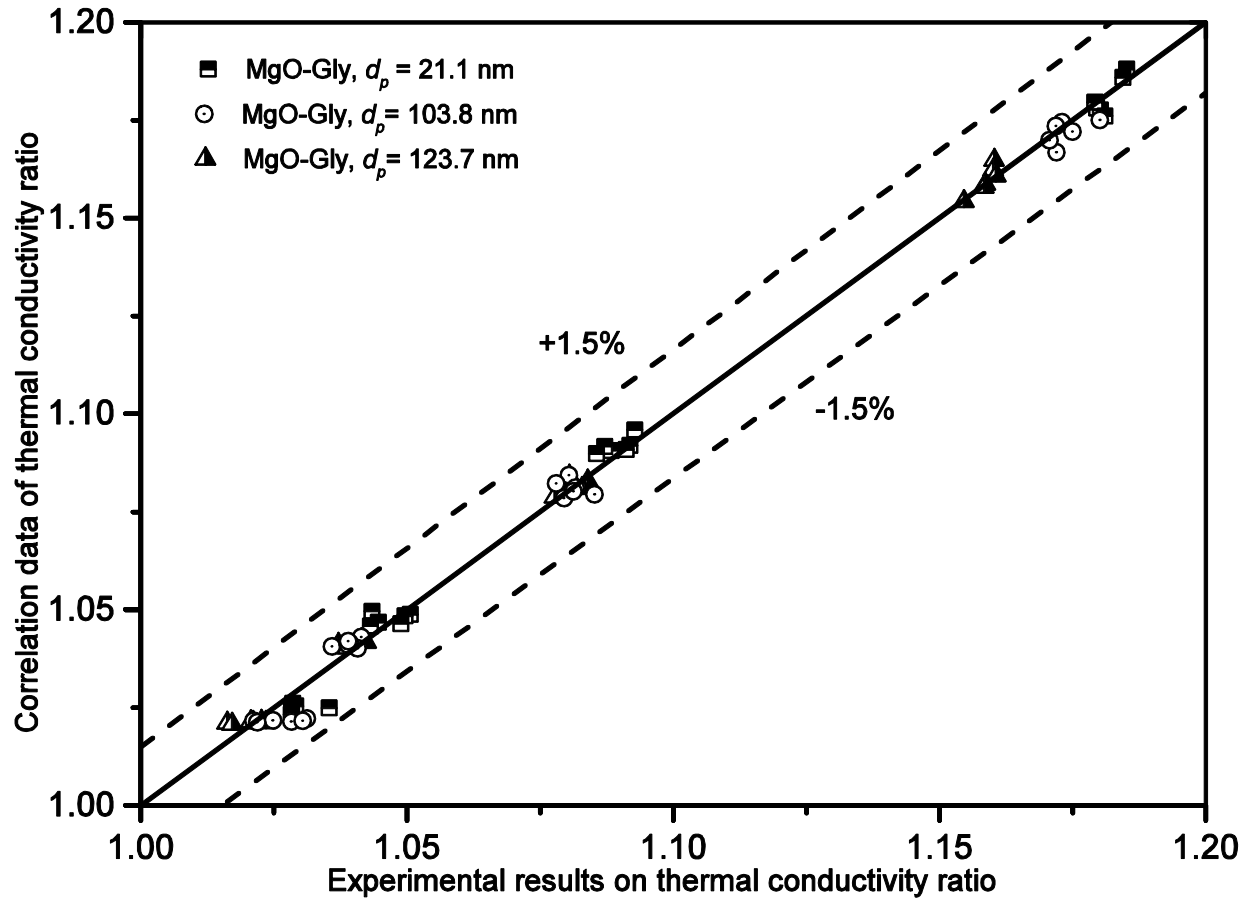
Figure 13: Comparison of the thermal conductivity ratio between the predicted values from the present correlation and the experiments data on MgO-glycerol nanofluids
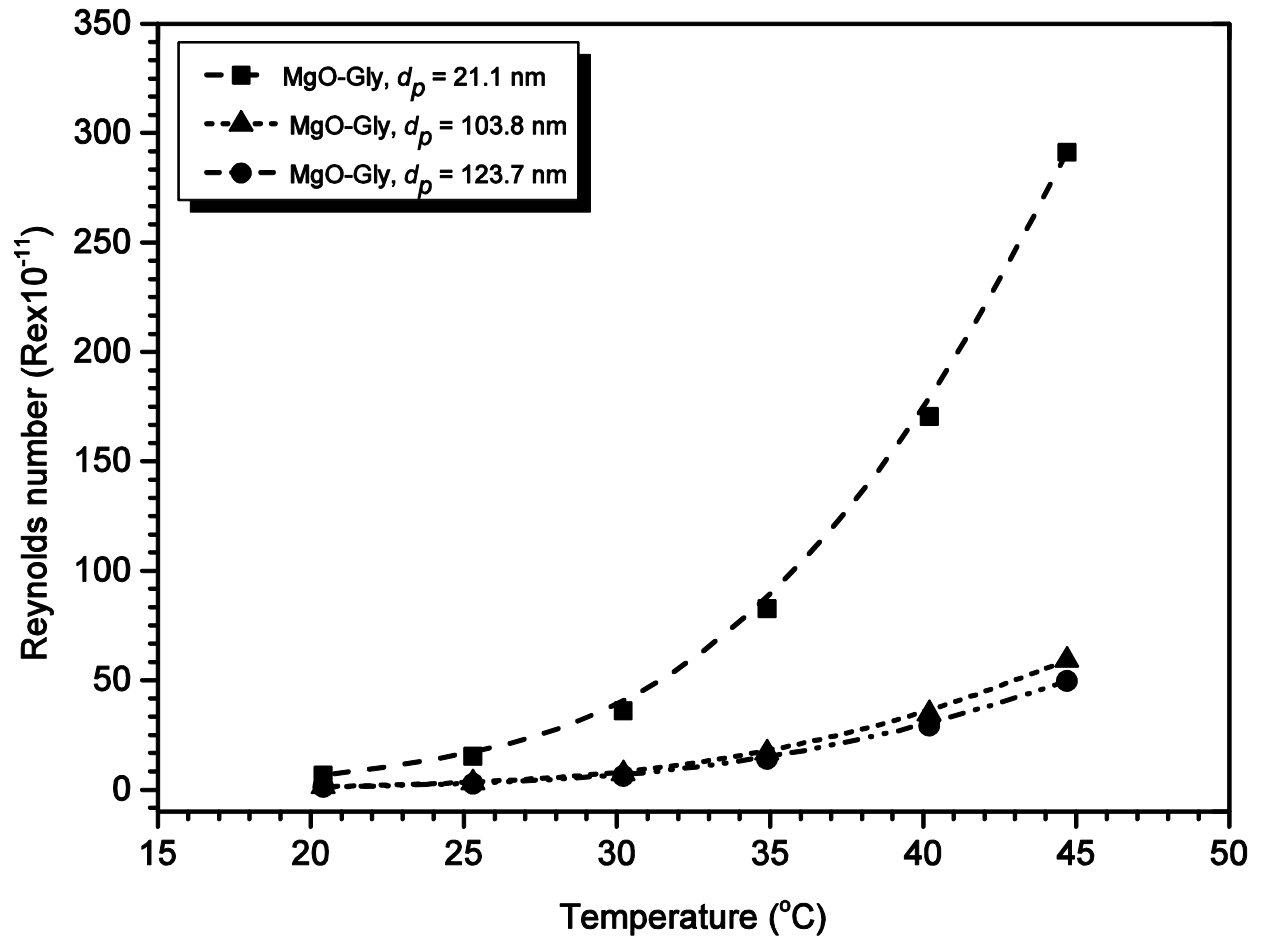
Figure 14: Reynolds number of different particle sizes of MgO-glycerol nanofluids
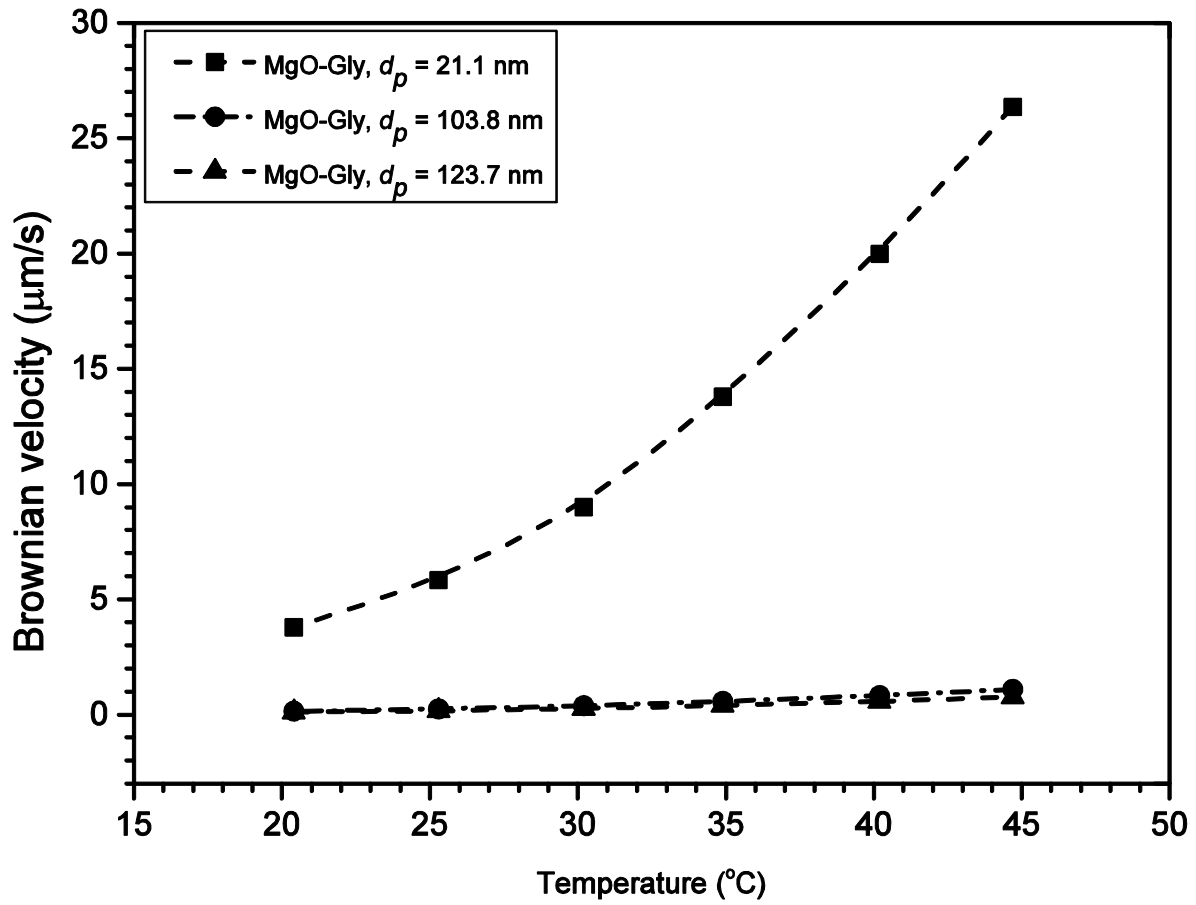
Figure 15: Brownian velocity of different particle sizes of MgO-glycerol nanofluids
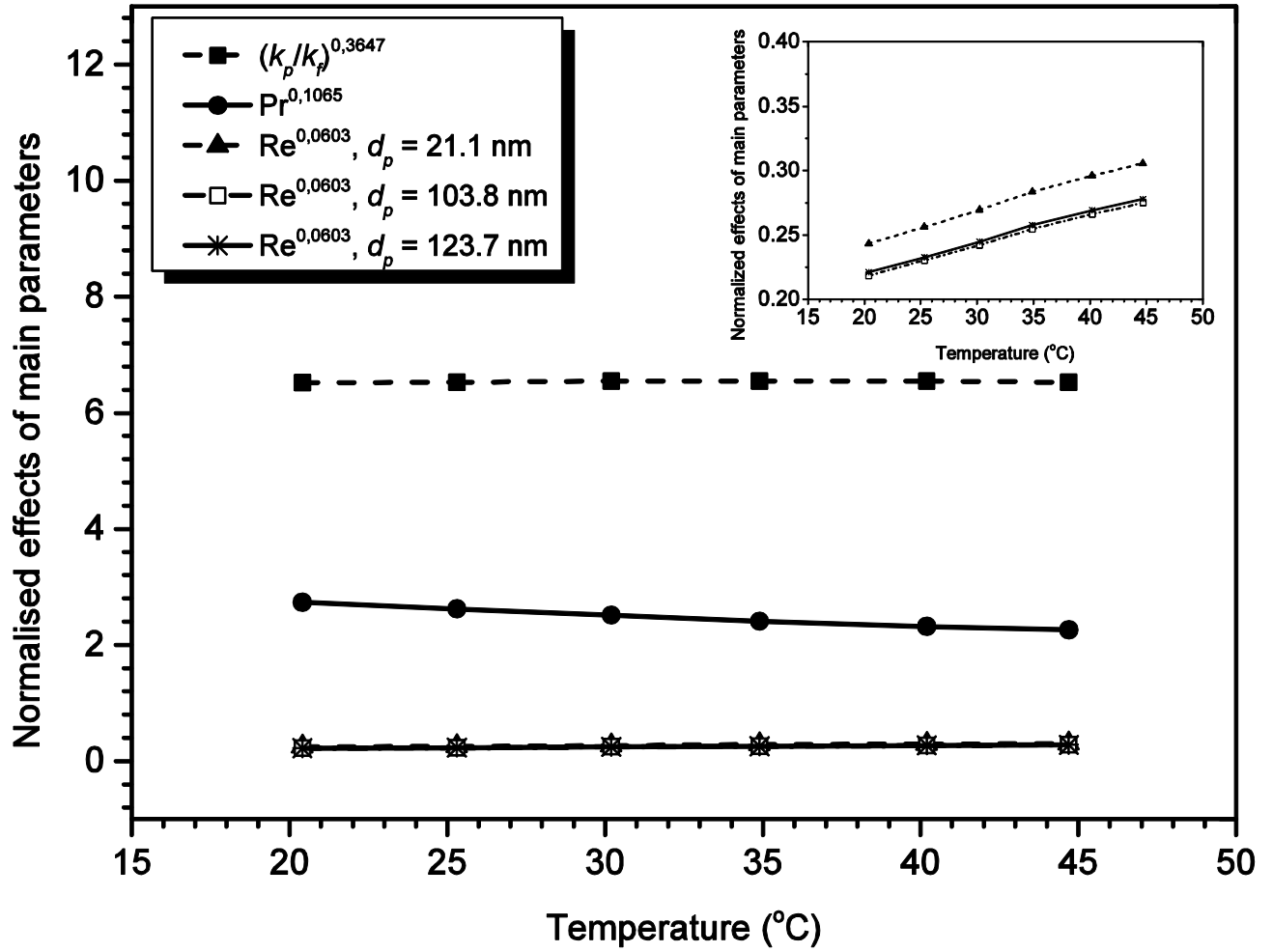
Figure 16: Temperature dependence of the normalised effects of the three parameters of the novel correlation of the MgO-glycerol nanofluids

Ntumba Tshimanga is currently completing his master's degree in Mechanical and Aeronautical Engineering at the University of Pretoria in South Africa. He obtained a BEng degree in Mining Engineering at Université de Mbujimayi in the Democratic Republic of Congo in 2004 and a BEng honours degree in Mining Engineering at the University of Pretoria, South Africa, in 2011.

Mohsen Sharifpur is a senior lecturer in the Department of Mechanical and Aeronautical Engineering at the University of Pretoria and is responsible for the Nanofluids Research Laboratory. He received a BSc (Mechanical Engineering) degree from Shiraz University in Iran. He completed an MSc degree in Nuclear Engineering, and received a full scholarship for his PhD study in Mechanical Engineering (thermal fluid) from Eastern Mediterranean University. He was the only postgraduate student who received four out of four for the cumulative grade point average (CGPA) when he received his PhD. He is the author and co-author of more than 50 articles and conference papers. His research interests include convective multiphase flow, thermal fluid behaviour of nanofluids, convection in porous media, computational fluid dynamics (CFD) and waste heat in thermal systems. He also reviews notable accredited journals.

Josua Meyer obtained his BEng degree cum laude in 1984, an MEng degree cum laude in 1986 and a PhD in 1988, all in mechanical engineering from the University of Pretoria. He is registered as a professional engineer. After his military service from 1988 to 1989, he accepted a position as associate professor in the Department of Mechanical Engineering at the erstwhile

Potchefstroom University for Christian Higher Education (now North-West University) in 1990. He was acting head and professor in this department until he accepted a position as professor in the Department of Mechanical and Manufacturing Engineering at the erstwhile Rand Afrikaans University (now the University of Johannesburg) in 1994. He was Chairman of the Department from 1999 until the end of June 2002, when he was appointed Professor and Head of the Department of Mechanical and Aeronautical Engineering at the University of Pretoria . Presently, he is the Chair of the School of Engineering at the University of Pretoria. He specialises in heat transfer, fluid mechanics and the thermodynamic aspects of heating, ventilation and air-conditioning. He is the author and co-author of more than 450 articles, conference papers and patents and he has received various prestigious awards for his research. He is also a fellow or member of various professional institutes and societies, such as the South African Institute for Mechanical Engineers, the South African Institute for Refrigeration and Air-Conditioning, the American Society for Mechanical Engineers, and the American Society of Heating, Refrigeration and Air-Conditioning Engineers. He is regularly invited as a keynote speaker at local and international conferences. He has received various teaching and exceptional achiever awards. He is an associate editor of *Heat Transfer Engineering* and editor of the *Journal of Porous Media*.